

Higgs boson pair production in non-linear Effective Field Theory with full m_t -dependence at NLO QCD

G. Buchalla,^a M. Capozzi,^b A. Celis,^a G. Heinrich,^b L. Scyboz^b

^a*Ludwig-Maximilians-Universität München, Fakultät für Physik, Arnold Sommerfeld Center for Theoretical Physics, 80333 München, Germany*

^b*Max Planck Institute for Physics, Föhringer Ring 6, 80805 München, Germany*

E-mail: gerhard.buchalla@physik.uni-muenchen.de,
mcapozi@mpp.mpg.de, alejandro.celis@physik.uni-muenchen.de,
gudrun@mpp.mpg.de, scyboz@mpp.mpg.de

ABSTRACT: We present a calculation of the NLO QCD corrections to Higgs boson pair production within the framework of a non-linearly realised Effective Field Theory in the Higgs sector, described by the electroweak chiral Lagrangian. We analyse how the NLO corrections affect distributions in the Higgs boson pair invariant mass and the transverse momentum of one of the Higgs bosons. We find that these corrections lead to significant and non-homogeneous K-factors in certain regions of the parameter space. We also provide an analytical parametrisation for the total cross-section and the m_{hh} distribution as a function of the anomalous Higgs couplings that includes NLO corrections. Such a parametrisation can be useful for phenomenological studies.

KEYWORDS: NLO computations, QCD phenomenology, Higgs, Effective Field Theory, future colliders

Contents

1	Introduction	1
2	Details of the calculation	4
2.1	The Higgs-electroweak chiral Lagrangian	4
2.2	Calculation of the NLO QCD corrections	6
2.2.1	Virtual corrections	11
2.2.2	Real radiation	11
2.2.3	Parametrisation of the total cross section	12
2.2.4	Validation of the calculation	12
3	Phenomenological results	12
3.1	NLO cross sections and heat maps	13
3.2	Cross sections and distributions at several benchmark points	17
3.2.1	Total cross sections	18
3.2.2	m_{hh} and $p_{T,h}$ distributions	19
3.2.3	Discussion of the benchmark points	28
4	Conclusions	29
A	Appendix	30
A.1	Differential coefficients of all coupling combinations for m_{hh}	30
A.2	Relation between EWChL and SMEFT	30
B	Erratum	33

1 Introduction

Exploring the Higgs sector and the mechanism of electroweak symmetry breaking is one of the primary goals for the current and future LHC program as well as other planned experiments. While some of the properties of the Higgs boson, like its mass, spin and couplings to electroweak bosons, have been measured meanwhile impressively well [1], other parameters, like the couplings to (light) fermions, and in particular the self-coupling, are still largely unconstrained and leave room for physics beyond the Standard Model, see e.g. Ref. [2] for a recent review.

In the Standard Model (SM) the strength of all Higgs boson couplings is predicted; however, effects of physics beyond the Standard Model (BSM) may lead to deviations which, once firmly established, are a clear sign of New Physics. Since higher-order QCD corrections are known to be important in Higgs boson production processes, they need to be taken into account to improve the sensitivity to New Physics effects.

Given the energy gap between the electroweak scale at $v \simeq 250$ GeV and a New Physics scale Λ which is supposed to be in the TeV range, it is natural to parametrise the BSM effects in a model-independent way in an Effective Field Theory (EFT) framework. Such a framework can be formulated in various ways, where we can distinguish two main categories, often called “linear EFT” and “non-linear EFT”. The linear EFTs [3, 4], also known as “SMEFT” [5–9], are organised by canonical dimensions, formulated as power series in the dimensionful parameter $1/\Lambda$. The non-linear EFTs are organised by chiral dimensions. The corresponding formalism, including a light Higgs boson, has been developed in Refs. [10–23] and usually goes by the name “Electroweak Chiral Lagrangian” (EWChL). We will work in the “non-linear EFT” framework, where the Higgs field is an electroweak singlet. The main benefit of this approach is that the anomalous Higgs couplings are singled out, in a systematic way, as the dominant New Physics effects in the electroweak sector.

Higgs boson pair production in gluon fusion is the most promising process to find out whether the Higgs boson self-coupling is Standard-Model-like. Early studies of Higgs boson pair production within an EFT framework can be found in Refs. [24–27]. Many phenomenological investigations about the potential of this process to reveal New Physics have been performed since, see e.g. Refs. [28–44].

In the SM, Higgs boson pair production has been calculated at leading order in Refs. [45–47]. As it is a loop-induced process, higher order calculations with full top quark mass dependence involve multi-scale two-loop integrals. Therefore, the NLO calculations until recently have been performed in the $m_t \rightarrow \infty$ limit [48] also called HEFT (“Higgs Effective Field Theory”),¹ and then rescaled by a factor B_{FT}/B_{HEFT} , B_{FT} denoting the leading order matrix element squared in the full theory. This procedure is called “Born-improved HEFT” in the following. In Refs. [49, 50], an approximation called “FT_{approx}” was introduced, which contains the full top quark mass dependence in the real radiation, while the virtual part is calculated in the HEFT approximation and rescaled at the event level by the re-weighting factor B_{FT}/B_{HEFT} .

In addition, the HEFT results at NLO and NNLO have been improved by an expansion

¹Sometimes the electroweak chiral Lagrangian with a light Higgs boson is also referred to as *Higgs Effective Field Theory (HEFT)* in the literature. The two EFTs are unrelated and should be carefully distinguished. Here we employ the term *electroweak chiral Lagrangian* for the non-linear EFT of physics beyond the SM, and reserve the expression *HEFT* for the heavy-top limit in Higgs interactions.

in $1/m_t^2$ in Refs. [51–54]. The NNLO QCD corrections in the heavy-top limit have been computed in Refs. [52, 55–57], and they have been supplemented by an expansion in $1/m_t^2$ in Ref. [53] and by threshold resummation, at NLO+NNLL in Ref. [58] and at NNLO+NNLL in Ref. [59], leading to K-factors of about 1.2 relative to the Born-improved HEFT result.

The full NLO corrections, including the top quark mass dependence also in the virtual two-loop amplitudes, have been calculated in Ref. [60]. Phenomenological studies at 14 TeV and 100 TeV, including variations of the Higgs boson self-coupling, have been presented in Ref. [61]. The full NLO calculation was supplemented by NLL transverse momentum resummation in Ref. [62]. It also has been matched to parton shower Monte Carlo programs [63, 64], where the matched result of Ref. [63] is publicly available within the POWHEG-BOX-V2 framework.

Recent work also includes a combination of an analytic threshold expansion and a large- m_t expansion together with a Padé approximation framework [65], and analytic results based on a high energy expansion for the planar part of the two-loop amplitude [66]. Very recently, top quark mass effects have been incorporated in the NNLO HEFT calculation, including the full NLO result and combining one-loop double-real corrections with full top mass dependence with suitably reweighted real-virtual and double-virtual contributions evaluated in the large- m_t approximation [67].

Within a non-linear EFT framework, higher order QCD corrections have been performed in the $m_t \rightarrow \infty$ limit. The NLO QCD corrections have been calculated in Ref. [68], recently also supplemented with the case of CP-violating Higgs sectors [69]. The NNLO QCD corrections in the $m_t \rightarrow \infty$ limit including dimension 6 operators have been presented in Ref. [70]. These calculations found rather flat K-factors, which however could be an artefact of the $m_t \rightarrow \infty$ limit. One of the main goals of the present paper is to investigate whether this feature is preserved once the full top quark mass dependence is taken into account. We calculate the NLO QCD corrections to Higgs boson pair production in gluon fusion within the non-linear EFT framework, retaining the full top quark mass dependence, based on the numerical approach developed in Ref. [60]. In order to quantify the different effects of the five operators and corresponding couplings that can lead to deviations from the SM in the Higgs sector, we give results for the total NLO cross section parametrised in terms of 23 coefficients of all possible combinations of these couplings, as introduced at LO in Refs. [31, 71]. We also show differential distributions for 12 benchmark points which should be characteristic for clusters of BSM scenarios. Such clusters were identified in Refs. [71–73] at leading order and represent partitions of the BSM parameter space according to the shape of the differential distributions. We demonstrate that there are regions where the NLO corrections lead to substantial and non-homogenous K-factors and provide numbers

for the parametrisation of the NLO cross section, which can be used in subsequent phenomenological studies.

This paper is organised as follows. In Section 2, we explain the framework of the calculation. In particular, we introduce the Higgs-electroweak chiral Lagrangian and describe how it is applied to Higgs boson pair production, including the NLO QCD corrections. Section 3 is dedicated to the phenomenological results. We provide a parametrisation of the NLO cross section in terms of coefficients of all combinations of couplings occurring in the NLO cross section. Based on this parametrisation we show heat maps both at LO and at NLO, where we vary two couplings while keeping the others fixed to the SM values. Then we give results for total cross sections and differential distributions at twelve benchmark points and discuss their implications before we conclude. An appendix explains the conventions used for the tables containing the *differential* coefficients of the couplings in the Higgs boson pair invariant mass distribution. The values are available in `csv` format as ancillary files to the arXiv submission and the JHEP publication. A further appendix compares the treatment of Higgs-pair production in the Higgs-electroweak chiral Lagrangian and in SMEFT.

2 Details of the calculation

2.1 The Higgs-electroweak chiral Lagrangian

In the present analysis, we will describe the potential impact of physics beyond the Standard Model through the electroweak chiral Lagrangian including a light Higgs boson [19, 21, 74]. This framework provides us with a consistent effective field theory (EFT) for New Physics in the Higgs sector, as we will summarise in the following.

To leading order the Lagrangian is given by

$$\begin{aligned}
\mathcal{L}_2 = & -\frac{1}{2}\langle G_{\mu\nu}G^{\mu\nu}\rangle - \frac{1}{2}\langle W_{\mu\nu}W^{\mu\nu}\rangle - \frac{1}{4}B_{\mu\nu}B^{\mu\nu} + \sum_{\psi=q_L,l_L,u_R,d_R,e_R} \bar{\psi}i\not{D}\psi \\
& + \frac{v^2}{4} \langle D_\mu U^\dagger D^\mu U \rangle (1 + F_U(h)) + \frac{1}{2}\partial_\mu h \partial^\mu h - V(h) \\
& - v \left[\bar{q}_L \left(Y_u + \sum_{n=1}^{\infty} Y_u^{(n)} \left(\frac{h}{v} \right)^n \right) U P_+ q_R + \bar{q}_L \left(Y_d + \sum_{n=1}^{\infty} Y_d^{(n)} \left(\frac{h}{v} \right)^n \right) U P_- q_R \right. \\
& \quad \left. + \bar{l}_L \left(Y_e + \sum_{n=1}^{\infty} Y_e^{(n)} \left(\frac{h}{v} \right)^n \right) U P_- l_R + \text{h.c.} \right] . \tag{2.1}
\end{aligned}$$

The first line is the unbroken SM, the remainder represents the Higgs sector. Here h is the Higgs field and $U = \exp(2i\varphi^a T^a/v)$ encodes the electroweak Goldstone fields

φ^a , with T^a the generators of $SU(2)$. v is the electroweak vacuum expectation value, $P_{\pm} = 1/2 \pm T_3$, and

$$D_{\mu}U = \partial_{\mu}U + igW_{\mu}U - ig'B_{\mu}UT_3. \quad (2.2)$$

The trace of a matrix A is denoted by $\langle A \rangle$. The left-handed doublets of quarks and leptons are written as q_L and l_L , the right-handed singlets as u_R , d_R , e_R . Generation indices are omitted. In the Yukawa terms the right-handed quark and lepton fields are collected into $q_R = (u_R, d_R)^T$ and $l_R = (0, e_R)^T$, respectively. In general, different flavour couplings $Y_{u,d,e}^{(n)}$ can arise at every order in the Higgs field h^n , in addition to the usual Yukawa matrices $Y_{u,d,e}$. The h -dependent functions are

$$F_U(h) = \sum_{n=1}^{\infty} f_{U,n} \left(\frac{h}{v} \right)^n, \quad V(h) = v^4 \sum_{n=2}^{\infty} f_{V,n} \left(\frac{h}{v} \right)^n. \quad (2.3)$$

In the limit where

$$f_{U,1} = 2, \quad f_{U,2} = 1, \quad f_{V,2} = f_{V,3} = \frac{m_h^2}{2v^2}, \quad f_{V,4} = \frac{m_h^2}{8v^2}, \quad Y_f^{(1)} = Y_f, \quad (2.4)$$

and all other couplings $f_{U,n}$, $f_{V,n}$, $Y_f^{(n)}$ equal to zero, the Lagrangian in (2.1) reduces to the usual SM. For generic values of those parameters, the Lagrangian describes the SM with arbitrary modifications in the Higgs couplings. While the deviations of these couplings from their SM values could, in principle, be of order unity, the parametrisation in (2.1) remains relevant as long as the anomalous Higgs couplings are the dominant New Physics effects at electroweak energies. Employing (2.1), we assume that this is the case. Such a hypothesis remains to be tested experimentally. We emphasise, however, that the assumption is well motivated by the current status of Higgs coupling measurements. These still allow deviations from the SM of 10–20% or more, considerably larger than the typical precision of 1% reached in the electroweak gauge sector [75]. A useful property of the Lagrangian (2.1) is therefore that it allows us to concentrate on anomalous Higgs couplings in a systematic way [22, 76].

In fact, the intuitive picture of introducing (2.1) as the SM with modified Higgs couplings can be formulated as a consistent EFT. Because of the need to write the modified Higgs couplings in a gauge-invariant way, the Higgs field has to be represented as an electroweak singlet h , independent of the Goldstone matrix $U = \exp(2i\varphi^a T^a/v)$. The latter transforms as $U \rightarrow g_L U g_Y^{\dagger}$ under the SM gauge group. The symmetry is non-linearly realised on the Goldstone fields φ^a . The Lagrangian (2.1) is then non-renormalisable (in the traditional sense) as it contains interaction terms of arbitrary canonical dimension. The EFT is therefore not organised by the canonical dimension of operators, but rather by *chiral counting* in analogy to the chiral perturbation of pions

in QCD. Chiral counting is equivalent to an expansion in loop orders L , which can be conveniently counted by assigning *chiral dimensions* $d_\chi \equiv 2L + 2$ to fields and weak couplings. This assignment is simply 0 for bosons, and 1 for each derivative, fermion bilinear and weak coupling:

$$d_\chi(A_\mu, \varphi, h) = 0, \quad d_\chi(\partial, \bar{\psi}\psi, g, y) = 1. \quad (2.5)$$

Here A_μ represents a generic gauge field, φ the Goldstone bosons, and h the Higgs scalar. g denotes any of the SM gauge couplings g, g', g_s , and y any other weak coupling, such as the Yukawa couplings or the square-roots of the parameters $f_{V,n}$ in the Higgs potential.

Based on this counting, the leading-order expression (2.1) can be constructed from the SM field content and symmetries as the most general Lagrangian of chiral dimension 2. Leading processes are described by tree-level amplitudes from (2.1). Next-to-leading order effects come from one-loop contributions of (2.1) and from tree-level terms of the NLO Lagrangian \mathcal{L}_4 . Both are considered to be of ‘one-loop order’, or chiral dimension $d_\chi = 4$.

We next apply this framework to Higgs-pair production $gg \rightarrow hh$. Since this process is loop-induced, at leading order both one-loop diagrams built from the LO interactions, as well as tree contributions from the NLO Lagrangian have to be taken into account. The relevant terms from the effective Lagrangian $\mathcal{L}_2 + \mathcal{L}_4$ are given by [77]

$$\mathcal{L} \supset -m_t \left(c_t \frac{h}{v} + c_{tt} \frac{h^2}{v^2} \right) \bar{t}t - c_{hhh} \frac{m_h^2}{2v} h^3 + \frac{\alpha_s}{8\pi} \left(c_{ggh} \frac{h}{v} + c_{gggh} \frac{h^2}{v^2} \right) G_{\mu\nu}^a G^{a,\mu\nu}. \quad (2.6)$$

The first three couplings, c_t, c_{tt}, c_{hhh} , are from \mathcal{L}_2 , the Higgs-gluon couplings c_{ggh} and c_{gggh} from \mathcal{L}_4 [19, 76]. To lowest order in the SM $c_t = c_{hhh} = 1$ and $c_{tt} = c_{ggh} = c_{gggh} = 0$. In general, all couplings may have arbitrary values of $\mathcal{O}(1)$. Note that we have extracted a loop factor from the definition of the Higgs-gluon couplings.

The leading-order diagrams are shown in Fig. 1. All diagrams are at the same order in the chiral counting (chiral dimension 4, equivalent to one-loop order). They illustrate the interplay between leading order anomalous couplings (black dots) within loops, and next-to-leading order terms (black squares) at tree level. All the five couplings defined in (2.6) appear in Fig. 1. In the following section we discuss the extension of this analysis to the next order in QCD.

2.2 Calculation of the NLO QCD corrections

Within the framework of the electroweak chiral Lagrangian, the calculation of the $gg \rightarrow hh$ amplitude can be extended to the next order in the loop expansion, that is

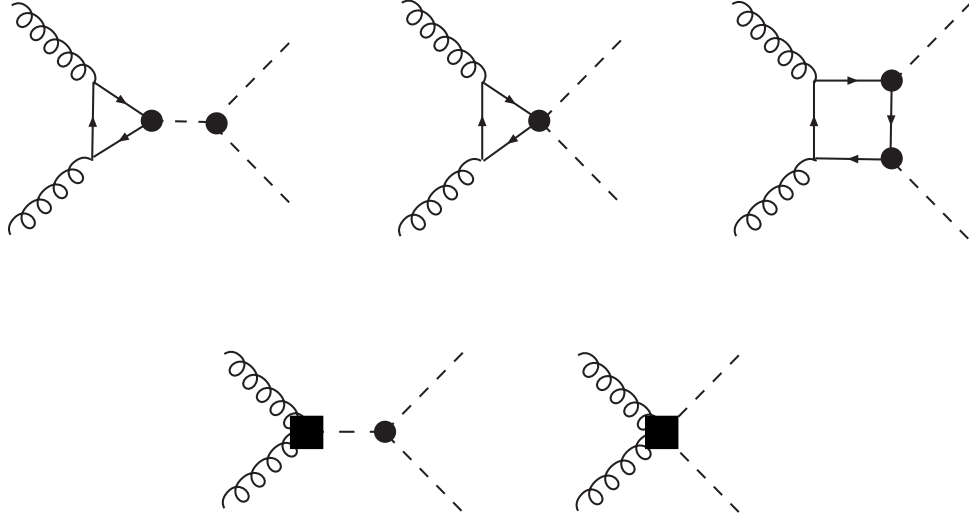


Figure 1: Higgs-pair production in gluon fusion at leading order in the chiral Lagrangian. The black dots indicate vertices from \mathcal{L}_2 , the black squares denote local terms from \mathcal{L}_4 .

to two-loop order, or chiral dimension 6. In full generality, this would require to also include two-loop electroweak corrections and local terms from the Lagrangian at chiral dimension 6. The latter introduce additional couplings, parametrising subleading new-physics effects. Such effects are beyond the experimental sensitivity in the foreseeable future, given that even the determination of the LO couplings in (2.6) remains a substantial challenge. On the other hand, radiative corrections from QCD are known to be very important for $gg \rightarrow hh$ and similar processes.

For this reason, we extend the calculation of $gg \rightarrow hh$ to the next order in the non-linear EFT, but restrict the NLO corrections to the effects from QCD. Within the systematics of the EWChL this approximation corresponds to including those corrections at chiral dimension 6 that come with a relative factor of the QCD coupling g_s^2 . This procedure is consistent without introducing further anomalous couplings, beyond the ones in (2.6), because this effective Lagrangian is renormalisable with respect to QCD [22]. Since the LO amplitude for $gg \rightarrow hh$ scales as $\sim g_s^2$, the NLO virtual corrections of interest to us comprise all the diagrams at two-loop order carrying a factor of g_s^4 . They exist as two-loop, one-loop and tree topologies, as illustrated in Figs. 2, 3 and 4, respectively. In addition, real emission diagrams at $\mathcal{O}(g_s^3)$ have to be included as shown in Fig. 5. To further clarify our approximation with respect to the full chiral expansion at NLO, we give in Fig. 6 a few examples of higher-order effects that are consistently neglected

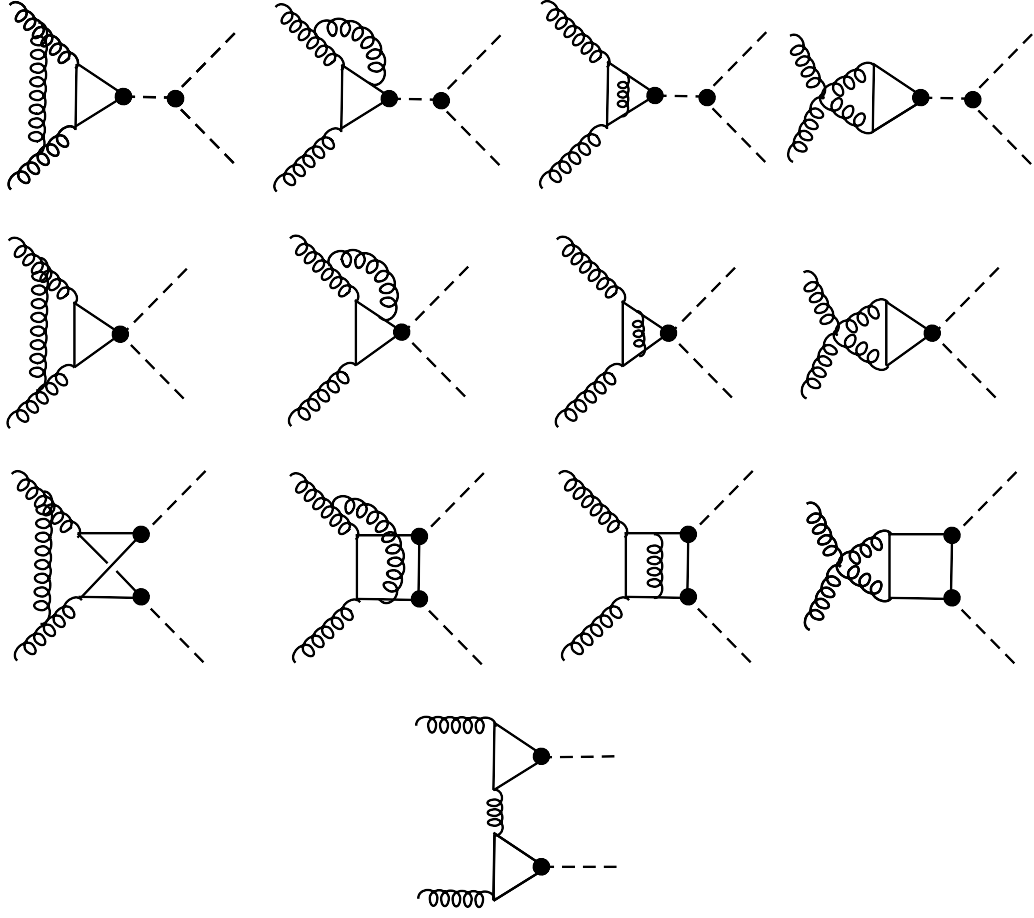


Figure 2: Higgs-pair production in gluon fusion at NLO: Examples for virtual two-loop diagrams at order g_s^4 .

in our scheme:

Example (a) shows a correction from electroweak-boson exchange. It is of two-loop order, but scales as $g_s^2 g^2$, rather than g_s^4 . It is not a NLO QCD effect and we neglect it here.

Similarly, the one-loop topology in (b) counts as two-loop order, but scales only as $g_s^2 c_{hhhh}$, with c_{hhhh} the (anomalous) quartic Higgs coupling.

In example (c) we consider an anomalous top-gluon coupling of the form $Q_{tG} = y_t g_s \bar{t}_L \sigma_{\mu\nu} G^{\mu\nu} t_R$, where the top Yukawa coupling reflects the change in chirality. This operator is therefore (at least) of chiral dimension 4 (one-loop order) and the diagram in Fig. 6 (c) of two-loop order, but again not of order g_s^4 . Since (2.1) assumes that the top quark is weakly coupled to the (possibly strongly interacting) new-physics sector,

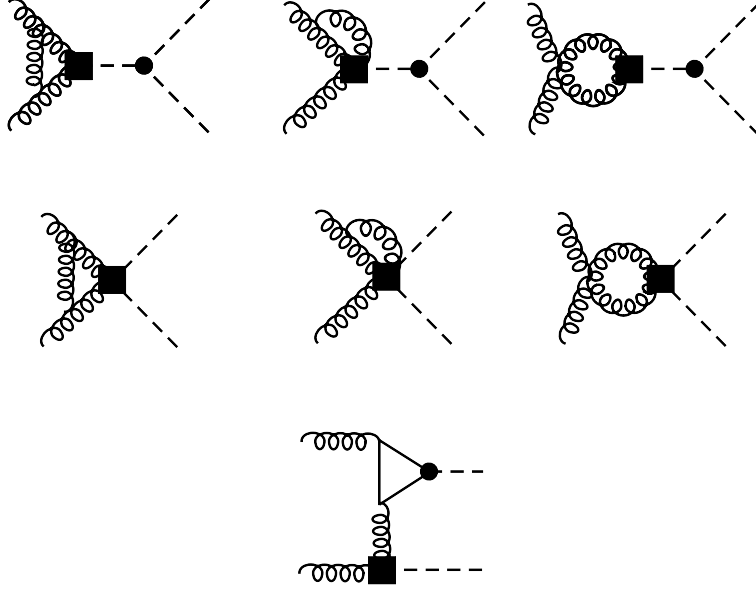


Figure 3: Higgs-pair production in gluon fusion at NLO: Examples for virtual one-loop diagrams at order g_s^4 .

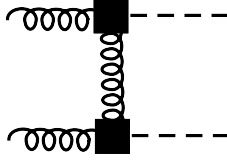


Figure 4: Higgs-pair production in gluon fusion at NLO: Tree diagram at order g_s^4 .

it is more likely that the operator comes with further weak couplings from t_L and t_R and thus carries chiral dimension 6. In this case, diagram (c) is of three-loop order and clearly negligible. The effect of the chromomagnetic operator on single Higgs boson production has been calculated recently in the context of SMEFT in Ref. [78].

Example (d) illustrates the effect of a local Higgs-gluon interaction of chiral dimension 6, which enters at two-loop order as a tree-level topology. A possible operator would be $g_s^2 G_{\mu\nu}^a G^{a,\mu\nu} \partial_\lambda h \partial^\lambda h$. However, this effect, although of two-loop order, does not scale as g_s^4 .

Finally, we may have an operator $g_s^3 f^{abc} G_{\mu\nu}^a G^{b,\nu}_\lambda G^{c,\lambda\mu} h$, also of chiral dimension 6. Diagram (e) then amounts to a two-loop order interaction with real emission, which is

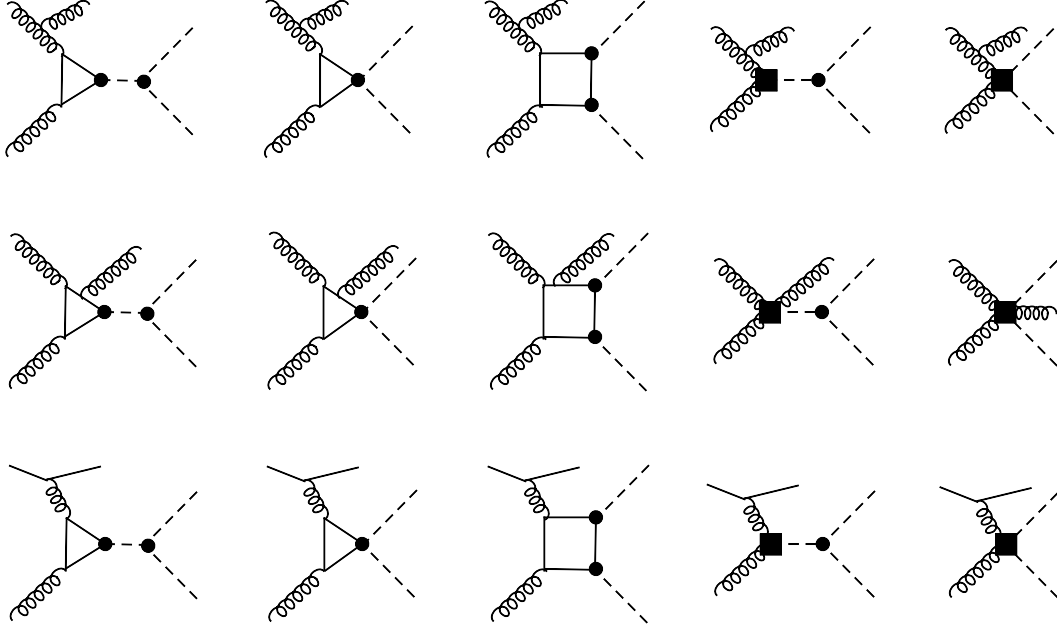


Figure 5: Higgs-pair production in gluon fusion at NLO: Examples for real-emission diagrams at order g_s^3 .

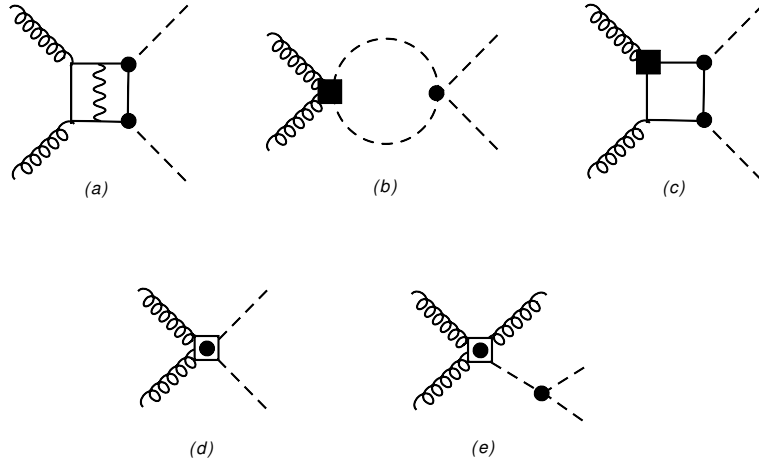


Figure 6: Higgs-pair production in gluon fusion at NLO: Examples for contributions that are consistently neglected within our approximation. The dotted square indicates a local term at chiral dimension 6 (two-loop order). See text for further explanation.

beyond our approximation.

At the technical level, the NLO QCD corrections have been calculated building on the

setup described in Refs. [60, 61], summarised briefly below.

2.2.1 Virtual corrections

The virtual part of order α_s^3 consists of genuine two-loop diagrams as well as one-loop and tree-level diagrams, see Figs. 2, 3 and 4.

For the two-loop part, we made use of the numerical results for the two-loop virtual diagrams in the Standard Model (SM) by dividing them into two classes: diagrams containing the Higgs-boson self-coupling (“triangle-type”), and diagrams without (“box-type”). The $t\bar{t}hh$ coupling generates new two-loop topologies, see e.g. the second line of Fig. 2. The results for these diagrams however can be obtained from the SM triangle-type diagrams by multiplying them with the inverse Higgs boson propagator and rescaling the couplings, i.e. multiplying with $c_{t\bar{t}}/c_{hh}$. The other two-loop diagrams occurring in our calculation have the same topologies as in the SM and therefore can be derived from the SM results by rescaling of the couplings c_t and c_{hh} .

The one-loop part containing the Higgs-gluon contact interactions has been calculated in two ways: first, using GOSAM [79, 80] in combination with a model file in UFO format [81], derived from an effective Lagrangian using FEYNRULES [82], and second analytically as a cross-check.

As we are only considering QCD corrections, the renormalisation procedure is the same as in the SM and is described in Ref. [61].

2.2.2 Real radiation

The real corrections consist of 5-point one-loop topologies with closed top quark loops as well as tree-level diagrams, see Fig. 5. Both classes of diagrams have been generated with GOSAM and arranged such that interferences between the two classes are properly taken into account.

In order to isolate the singularities due to unresolved radiation, we use the same framework as in Ref. [61], i.e. we use the Catani-Seymour dipole formalism [83], combined with a phase space restriction parameter α as suggested in Ref. [84].

The various building blocks are assembled in a C++ program and integrated over the phase space using the VEGAS algorithm [85] as implemented in the CUBA library [86].

2.2.3 Parametrisation of the total cross section

To parametrise the deviations of the total cross section from the one in the SM, we write the LO cross section in terms of the 15 coefficients A_1, \dots, A_{15} , following Refs. [31, 71].

$$\begin{aligned} \sigma/\sigma_{SM} = & A_1 c_t^4 + A_2 c_{tt}^2 + A_3 c_t^2 c_{hhh}^2 + A_4 c_{ggh}^2 c_{hhh}^2 + A_5 c_{gghh}^2 + A_6 c_{tt} c_t^2 + A_7 c_t^3 c_{hhh} \\ & + A_8 c_{tt} c_t c_{hhh} + A_9 c_{tt} c_{ggh} c_{hhh} + A_{10} c_{tt} c_{gghh} + A_{11} c_t^2 c_{ggh} c_{hhh} + A_{12} c_t^2 c_{gghh} \\ & + A_{13} c_t c_{hhh}^2 c_{ggh} + A_{14} c_t c_{hhh} c_{gghh} + A_{15} c_{ggh} c_{hhh} c_{gghh} . \end{aligned} \quad (2.7)$$

At NLO the coefficients A_1, \dots, A_{15} are modified and new terms appear. We find:

$$\begin{aligned} \Delta\sigma/\sigma_{SM} = & A_{16} c_t^3 c_{ggh} + A_{17} c_t c_{tt} c_{ggh} + A_{18} c_t c_{ggh}^2 c_{hhh} + A_{19} c_t c_{ggh} c_{gghh} \\ & + A_{20} c_t^2 c_{ggh}^2 + A_{21} c_{tt} c_{ggh}^2 + A_{22} c_{ggh}^3 c_{hhh} + A_{23} c_{ggh}^2 c_{gghh} . \end{aligned} \quad (2.8)$$

2.2.4 Validation of the calculation

To validate our results, we have compared the Born-improved NLO HEFT results calculated with our setup with the ones from Ref. [68], where we find agreement if we use $\mu_r = \mu_f = m_{hh}$ and MSTW2008 [87] PDFs at LO/NLO for the LO/NLO calculation, along with the corresponding α_s value.²

We also have cross-checked the results by using two independent codes, where the only common parts are the UFO model files and the SM virtual two-loop corrections.

In addition, we have compared the leading order distributions, benchmark points and fits of the coupling coefficients in the total cross section (see Eq. (2.7)) with the ones given in Refs. [31, 71, 72]. We find agreement with Ref. [31] for all A_i coefficients at the 1% level. Comparing to Refs. [71, 72], we systematically find values that differ by 15-20% for coefficients linear in c_{ggh} and by $\sim 40\%$ for the coefficient quadratic in c_{ggh} . We also compared our results with the distributions shown in Refs. [71, 72], finding agreement for all benchmark points except for benchmark point 8. While in Refs. [71, 72] a dip in the leading order distribution is found for benchmark point 8, we find no such dip. This is why we chose a different point of cluster 8 which does show a dip, and which we call 8a.

3 Phenomenological results

In this section we present numerical results for benchmark points which were identified in Ref. [71] to represent partitions of the BSM parameter space according to characteristic shapes of differential distributions, in particular the Higgs boson pair invariant mass distributions. All our results are for a centre-of-mass energy of $\sqrt{s} = 14$ TeV.

²Our default settings are to use PDF4LHC15 [88] PDFs for both the LO and the NLO results.

The results were computed using the PDF4LHC15_nlo_100_pdfas [88–91] parton distribution functions interfaced via LHAPDF [92], along with the corresponding value for $\alpha_s(\mu)$, with $\alpha_s(M_Z) = 0.118$. The masses of the Higgs boson and the top quark have been set to $m_h = 125$ GeV and $m_t = 173$ GeV (pole mass), respectively. The widths of the top quark (and the Higgs boson) have been set to zero. Bottom quarks are treated as massless and therefore are not included in the fermion loops. The scale uncertainties are estimated by varying the factorisation scale μ_F and the renormalisation scale μ_R around the central scale $\mu_0 = m_{hh}/2$, using the envelope of a 7-point scale variation. The latter means that we use $\mu_{R,F} = c_{R,F} \mu_0$, where $c_R, c_F \in \{2, 1, 0.5\}$, and consider each combination except the two extreme ones $c_R = 0.5, c_F = 2$ and $c_R = 2, c_F = 0.5$. In the SM case, the combinations $c_R = c_F = 0.5$ and $c_R = c_F = 2$ always coincided with the envelope of the 7 combinations to vary c_R, c_F .

3.1 NLO cross sections and heat maps

In this section we will provide results for the coefficients defined in Eqs. (2.7) and (2.8), i.e. for the expression

$$\begin{aligned} \sigma^{\text{NLO}}/\sigma_{SM}^{\text{NLO}} = & A_1 c_t^4 + A_2 c_{tt}^2 + A_3 c_t^2 c_{hhh}^2 + A_4 c_{ggh}^2 c_{hhh}^2 + A_5 c_{gghh}^2 + A_6 c_{tt} c_t^2 + A_7 c_t^3 c_{hhh} \\ & + A_8 c_{tt} c_t c_{hhh} + A_9 c_{tt} c_{ggh} c_{hhh} + A_{10} c_{tt} c_{gghh} + A_{11} c_t^2 c_{ggh} c_{hhh} + A_{12} c_t^2 c_{gghh} \\ & + A_{13} c_t c_{hhh}^2 c_{ggh} + A_{14} c_t c_{hhh} c_{gghh} + A_{15} c_{ggh} c_{hhh} c_{gghh} \\ & + A_{16} c_t^3 c_{ggh} + A_{17} c_t c_{tt} c_{ggh} + A_{18} c_t c_{ggh}^2 c_{hhh} + A_{19} c_t c_{ggh} c_{gghh} \\ & + A_{20} c_t^2 c_{ggh}^2 + A_{21} c_{tt} c_{ggh}^2 + A_{22} c_{ggh}^3 c_{hhh} + A_{23} c_{ggh}^2 c_{gghh}. \end{aligned} \quad (3.1)$$

We evaluated the coefficients in two different ways: determination via projections and performing a fit, finding agreement of the results within their uncertainties. The results of the projection method, including uncertainties, are summarised in Table 1.

In the following we show heat maps for the ratio σ/σ_{SM} , based on the results for A_1, \dots, A_{23} . For the fixed parameters the SM values are used. Further we use $\sigma_{SM}^{\text{LO}} = 19.85$ fb, $\sigma_{SM}^{\text{NLO}} = 32.95$ fb.

The couplings are varied in a range which seems reasonable when taking into account the current constraints on the Higgs coupling measurements [1, 93, 94], as well as recent limits on the di-Higgs production cross section [95–98].

In Fig. 7 we display heat maps where the anomalous coupling c_{tt} is varied in combination with the Higgs-gluon contact interactions c_{gghh} and c_{ggh} . We show the ratio to the SM total cross section both at LO and at NLO. We can see that the NLO corrections can lead to a significant shift in the iso-contours. It also becomes apparent that the cross sections are more sensitive to variations of c_{tt} than to variations of the contact interaction c_{ggh} .

A coeff	LO value	LO uncertainty	NLO value	NLO uncertainty
A_1	2.08059	0.00163127	2.23389	0.0100989
A_2	10.2011	0.00809032	12.4598	0.0424131
A_3	0.27814	0.00187658	0.342248	0.0153637
A_4	0.314043	0.000312416	0.346822	0.00327358
A_5	12.2731	0.0101351	13.0087	0.0962361
A_6	-8.49307	0.00885261	-9.6455	0.0503776
A_7	-1.35873	0.00148022	-1.57553	0.0136033
A_8	2.80251	0.0130855	3.43849	0.0771694
A_9	2.48018	0.0127927	2.86694	0.0772341
A_{10}	14.6908	0.0311171	16.6912	0.178501
A_{11}	-1.15916	0.00307598	-1.25293	0.0291153
A_{12}	-5.51183	0.0131254	-5.81216	0.134029
A_{13}	0.560503	0.00339209	0.649714	0.0287388
A_{14}	2.47982	0.0190299	2.85933	0.193023
A_{15}	2.89431	0.0157818	3.14475	0.148658
A_{16}			-0.00816241	0.000224985
A_{17}			0.0208652	0.000398929
A_{18}			0.0168157	0.00078306
A_{19}			0.0298576	0.000829474
A_{20}			-0.0270253	0.000701919
A_{21}			0.0726921	0.0012875
A_{22}			0.0145232	0.000703893
A_{23}			0.123291	0.00650551

Table 1: Results for the coefficients defined in Eq. (3.1). The uncertainties are obtained from the uncertainties on the total cross sections entering the projections, using error propagation which neglects correlations between these cross sections.

Fig. 8 shows variations of the triple Higgs coupling c_{hhh} in combination with c_{ggh} and c_{tt} . We observe that the deviations from the SM cross section can be substantial, and again we see a rapid variation of the cross section when changing c_{tt} .

In Fig. 9 we display variations of c_t versus c_{hhh} , and variations of c_t versus c_{tt} . We see that values of c_t around 2.0 in combination with large negative values of c_{hhh} can enhance the cross section by two orders of magnitude. Current experimental limits suggest that the total cross section for Higgs boson pair production does not exceed

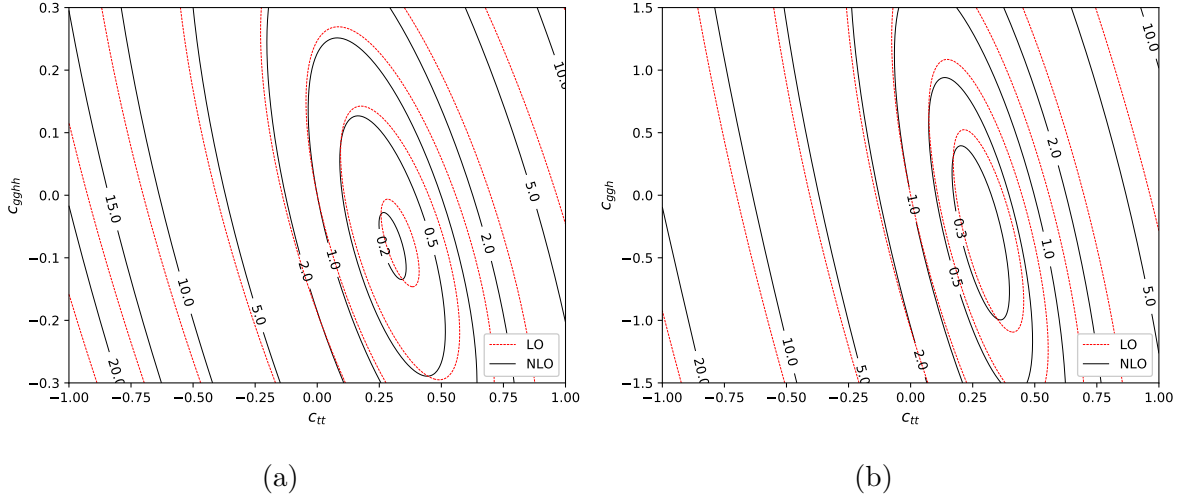


Figure 7: Iso-contours of σ/σ_{SM} : (a) c_{gghh} and (b) c_{ggh} versus c_{tt} .

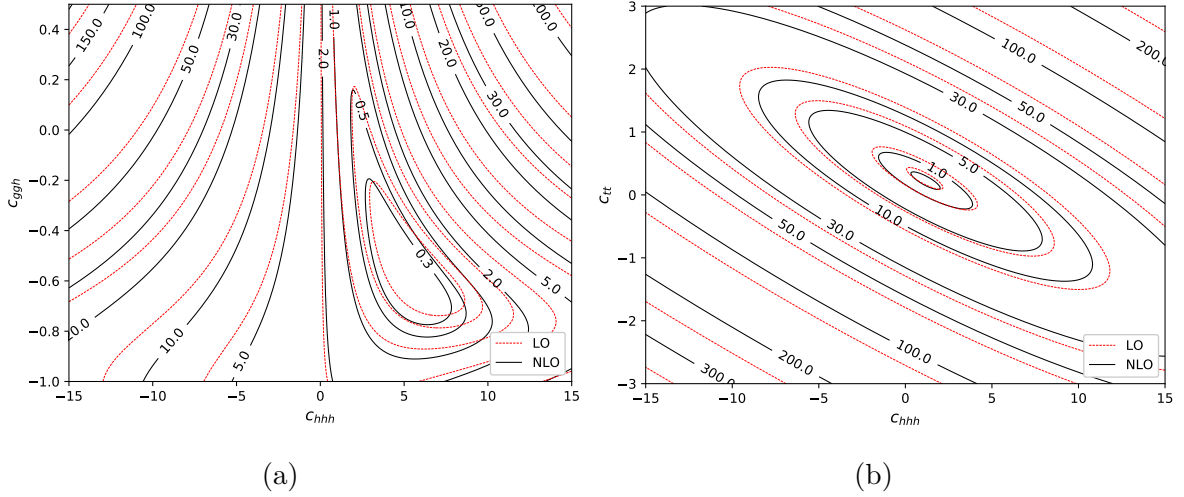


Figure 8: Iso-contours of σ/σ_{SM} : (a) c_{ggh} versus c_{hhh} and (b) c_{tt} versus c_{hhh} .

about 13–24 times the SM value, assuming a SM-like shape in the distributions [96, 97]. Together with the prospects that c_t will be increasingly well constrained in the future, e.g. from measurements of $t\bar{t}H$ production [99, 100], this should allow to constrain some of the parameter space for c_{hhh} .³ Fig. 10 shows variations of c_{gghh} versus c_{ggh} and

³Note that c_t and c_{ggh} already receive indirect constraints from single Higgs boson processes, as they enter in $gg \rightarrow h$ and $h \rightarrow \gamma\gamma$.

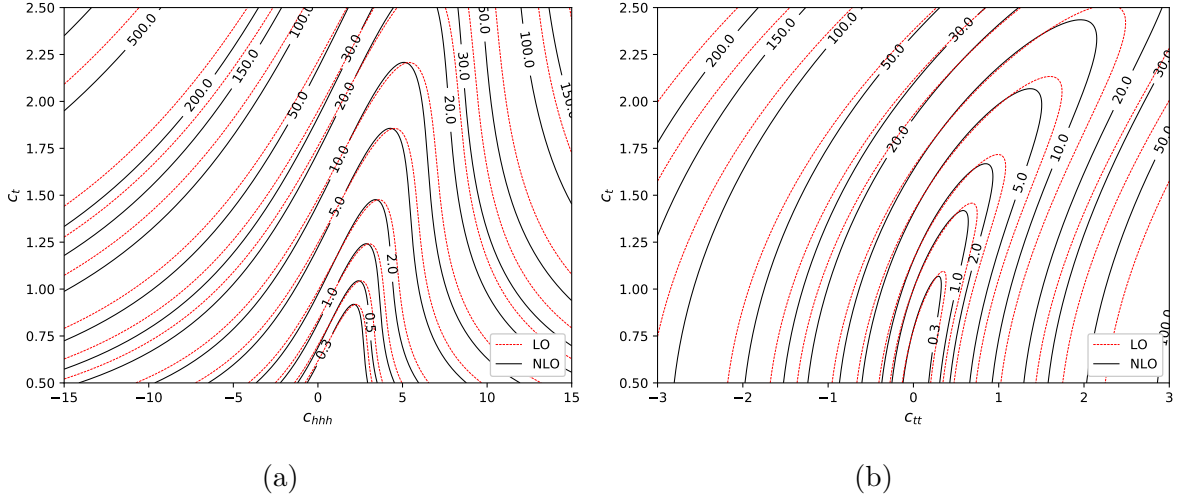


Figure 9: Iso-contours of σ/σ_{SM} : (a) c_t versus c_{hhh} and (b) c_t versus c_{tt} .

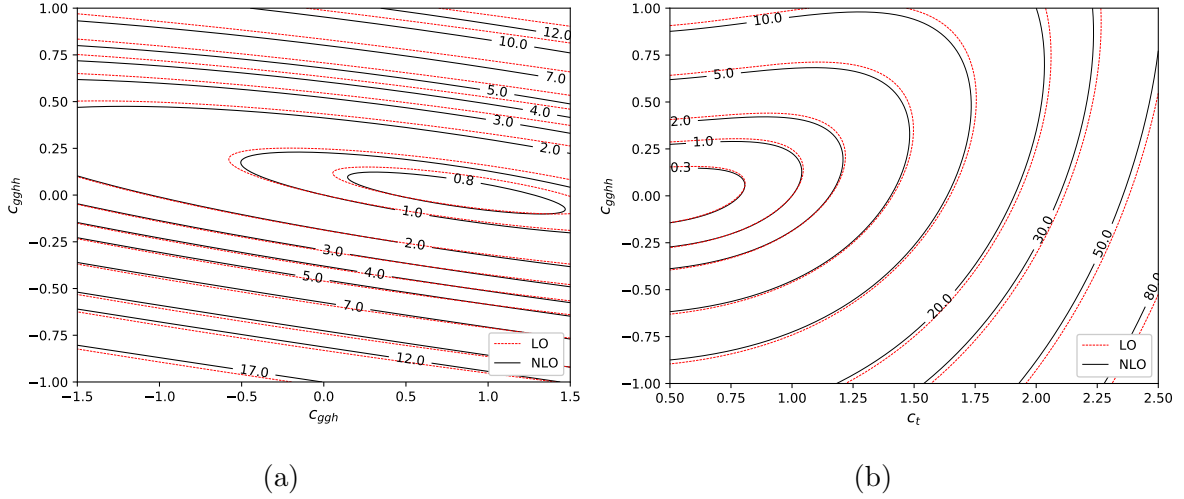


Figure 10: Iso-contours of σ/σ_{SM} : (a) c_{gghh} versus c_{ggh} and (b) c_{gghh} versus c_t .

c_t . We observe that the impact on the NLO corrections is milder in this case.

In Fig. 11 we show the K-factors as a function of the coupling parameters, with the others fixed to their SM values. It shows that the rather flat K-factors which have been found [68, 70] in the $m_t \rightarrow \infty$ limit (flat with respect to variations of one of the coupling parameters) show a much stronger dependence on the coupling parameters once the full top quark mass dependence is taken into account.

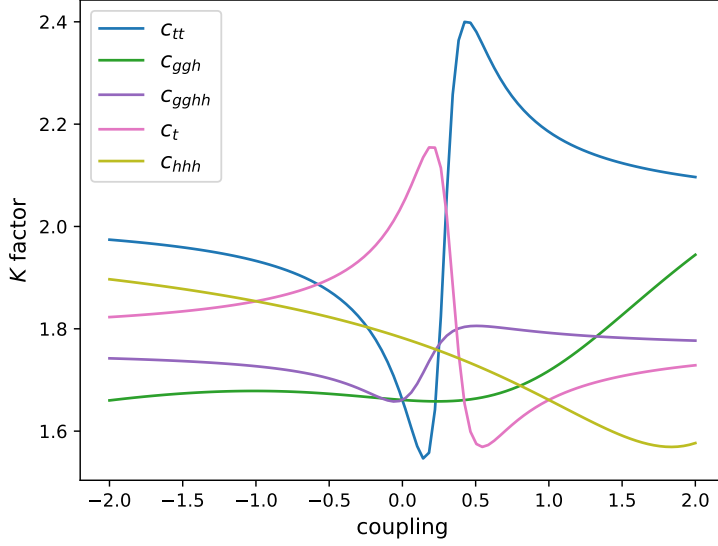


Figure 11: K-factors for the total cross section as a function of the different couplings.

3.2 Cross sections and distributions at several benchmark points

In the following we will show results for the benchmark points defined in Ref. [71], except for benchmark point 8, where we choose a different one (denoted as “outlier” number 5 for cluster 8 in Ref. [72]) which has a more characteristic shape, and which we call 8a.

The conventions for the definition of the couplings between our Lagrangian, given in Eq. (2.6), and the one of Ref. [71] are slightly different. In Table 2 we list the conversion factors to translate between the conventions.

EWChL Eq. (2.6)	Ref. [71]
c_{hhh}	κ_λ
c_t	κ_t
c_{tt}	c_2
c_{ggh}	$\frac{2}{3}c_g$
c_{gggh}	$-\frac{1}{3}c_{2g}$

Table 2: Translation between the conventions for the definition of the anomalous couplings.

The benchmark points translated to our conventions are given in Table 3.

Benchmark	c_{hhh}	c_t	c_{tt}	c_{ggh}	c_{gggh}
1	7.5	1.0	-1.0	0.0	0.0
2	1.0	1.0	0.5	$-\frac{1.6}{3}$	-0.2
3	1.0	1.0	-1.5	0.0	$\frac{0.8}{3}$
4	-3.5	1.5	-3.0	0.0	0.0
5	1.0	1.0	0.0	$\frac{1.6}{3}$	$\frac{1.0}{3}$
6	2.4	1.0	0.0	$\frac{0.4}{3}$	$\frac{0.2}{3}$
7	5.0	1.0	0.0	$\frac{0.4}{3}$	$\frac{0.2}{3}$
8a	1.0	1.0	0.5	$\frac{0.8}{3}$	0.0
9	1.0	1.0	1.0	-0.4	-0.2
10	10.0	1.5	-1.0	0.0	0.0
11	2.4	1.0	0.0	$\frac{2.0}{3}$	$\frac{1.0}{3}$
12	15.0	1.0	1.0	0.0	0.0
SM	1.0	1.0	0.0	0.0	0.0

Table 3: Benchmark points used for the distributions shown below.

3.2.1 Total cross sections

We first show the values for the total cross sections, together with their statistical uncertainties and the uncertainties from scale variations. We should point out that the cross sections for benchmark points B_3, B_4 and B_{12} are larger than the limits measured in the $b\bar{b}\gamma\gamma$ decay channel [97, 98]. However, within the same cluster [72], i.e. the set of couplings which lead to a similar *shape* of the m_{hh} distribution, one can easily find combinations of couplings where the value of the total cross section is below the experimental exclusion bound. For example, taking the point $c_{hhh} = 1, c_t = 1, c_{tt} = 0, c_{ggh} = 4/15, c_{gggh} = -0.2$ in cluster 4 leads to a cross section of about 1.8 times the SM cross section, still far from being excluded, see Fig. 16.

The large differences in the statistical uncertainties for the different benchmark points are due to the fact that the results for the virtual two-loop part are based on rescaling of the SM numerical results, which are distributed differently in the phase space. Therefore the statistical uncertainties are largest for benchmark points where the distribution in phase space is very different from the SM case. For example, benchmark 10 has a large differential cross section at low m_{hh} values, where the SM statistics is very low. This translates into the large statistical uncertainty for benchmark 10.

Benchmark	σ_{NLO} [fb]	K-factor	scale uncert. [%]	stat. uncert. [%]	$\frac{\sigma_{NLO}}{\sigma_{NLO,SM}}$
B_1	194.89	1.88	$^{+19}_{-15}$	1.6	5.915
B_2	14.55	1.88	$^{+5}_{-13}$	0.56	0.4416
B_3	1047.37	1.98	$^{+21}_{-16}$	0.15	31.79
B_4	8922.75	1.98	$^{+19}_{-16}$	0.39	270.8
B_5	59.325	1.83	$^{+4}_{-15}$	0.36	1.801
B_6	24.69	1.89	$^{+2}_{-11}$	2.1	0.7495
B_7	169.41	2.07	$^{+9}_{-12}$	2.2	5.142
B_{8a}	41.70	2.34	$^{+6}_{-9}$	0.63	1.266
B_9	146.00	2.30	$^{+22}_{-16}$	0.31	4.431
B_{10}	575.86	2.00	$^{+17}_{-14}$	3.2	17.48
B_{11}	174.70	1.92	$^{+24}_{-8}$	1.2	5.303
B_{12}	3618.53	2.07	$^{+16}_{-15}$	1.2	109.83
SM	32.95	1.66	$^{+14}_{-13}$	0.1	1

Table 4: Total cross sections at NLO (second column) including the K-factor (third column), scale uncertainties (4th column) and statistical uncertainties (5th column) and the ratio to the SM total NLO cross section (6th column).

3.2.2 m_{hh} and $p_{T,h}$ distributions

Now we consider differential cross sections for the 12 benchmark points. We show the Higgs boson pair invariant mass distribution and the transverse momentum distribution of one (any) of the Higgs bosons. For each benchmark point we show the full NLO result in red, and compare it to the two approximations “Born-improved NLO HEFT” (purple) and FT_{approx} (green). The leading order (yellow) as well as the SM results are also shown (blue NLO, black LO). The lower ratio plot shows the ratio of the two approximate results to the full NLO result. The upper ratio plot shows the differential BSM K-factor, i.e. $NLO_{\text{BSM}}/LO_{\text{BSM}}$, both evaluated with the same PDFs.

Fig. 12 corresponds to a benchmark point with no Higgs-gluon contact interactions, but an enhanced triple Higgs coupling and a nonzero $t\bar{t}hh$ interaction with $c_{t\bar{t}} < 0$. The total cross section is about 6 times the SM cross section, and the shape of the m_{hh} distribution is completely different from the SM. In fact, one can show analytically that the LO cross section in the $m_t \rightarrow \infty$ limit exactly vanishes near $m_{hh} = 364$ GeV, which relates to the dip in the distribution. The huge enhancement at low m_{hh} values is due to the large value of c_{hhh} .

Fig. 13, corresponding to benchmark 2, shows a very different behaviour. The result is

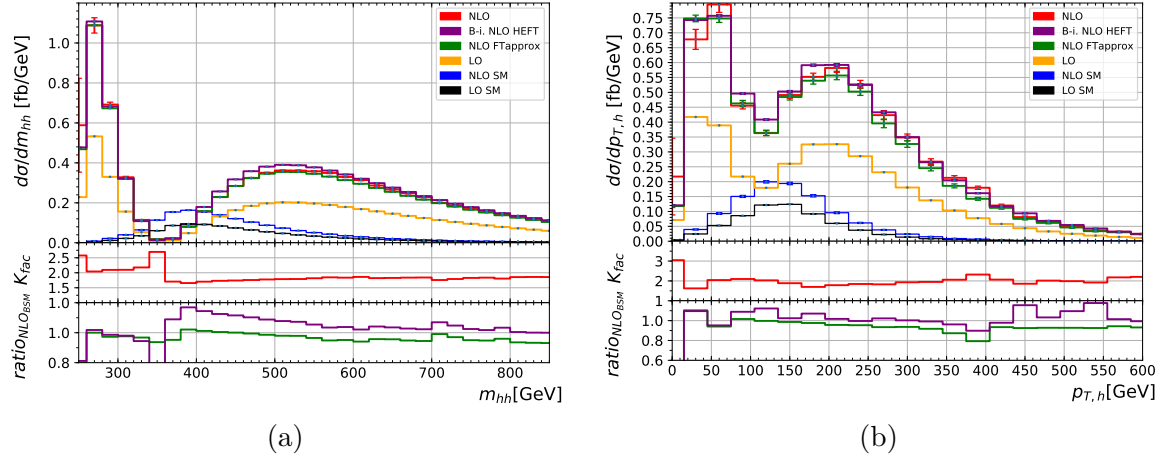


Figure 12: Higgs boson pair invariant mass distribution and transverse momentum distribution of one of the Higgs bosons for benchmark point 1, $c_{hhh} = 7.5$, $c_t = 1$, $c_{tt} = -1$, $c_{ggh} = c_{gghh} = 0$. The ratio plot with the K-factor shows $\text{NLO}_{\text{BSM}}/\text{LO}_{\text{BSM}}$. The lower ratio plot shows the ratios (Born-improved NLO HEFT)/ NLO_{BSM} (purple) and $\text{FT}_{\text{approx}}/\text{NLO}_{\text{BSM}}$ (green).

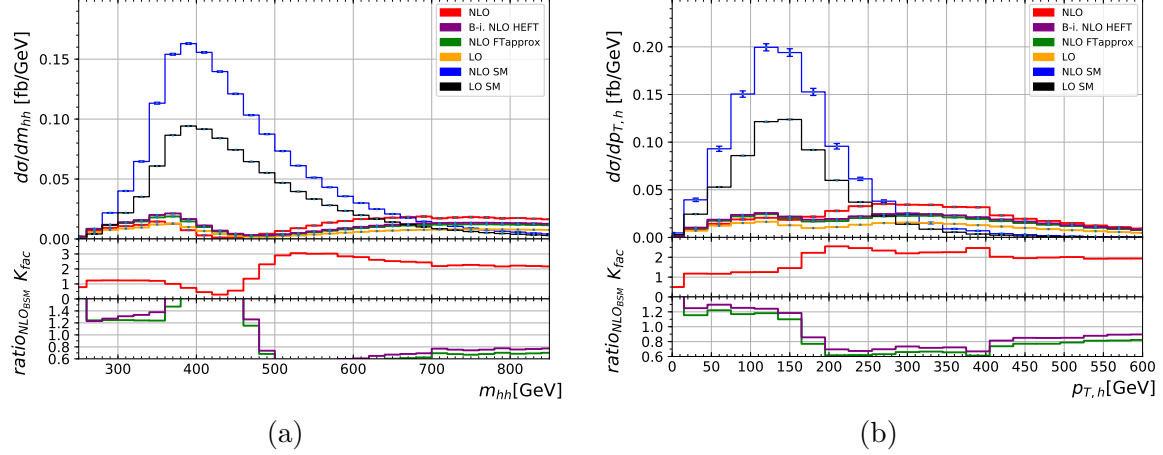


Figure 13: Same as Fig. 12 but for benchmark point 2, $c_{hhh} = 1$, $c_t = 1$, $c_{tt} = 0.5$, $c_{ggh} = -8/15$, $c_{gghh} = -0.2$.

very much suppressed in the region where the SM shows a peak, while there is a large enhancement in the tail of both the m_{hh} and the $p_{T,h}$ distributions. The enhancement in the tail is mainly due to the nonzero c_{gghh} value, as the amplitude proportional to c_{gghh} grows like \hat{s} [31]. We also notice that the approximations “Born-improved NLO HEFT” and $\text{FT}_{\text{approx}}$ cannot describe the pattern around the $2m_t$ threshold, where the

nonzero value of c_{tt} seems to play a significant role. The K-factor for benchmark 2 is very non-homogeneous around the dip in the m_{hh} distribution, and can reach up to a factor of three. This is a clear example where rescaling the LO result with a K-factor obtained from higher order calculations in the HEFT approximation would lead to very different results.

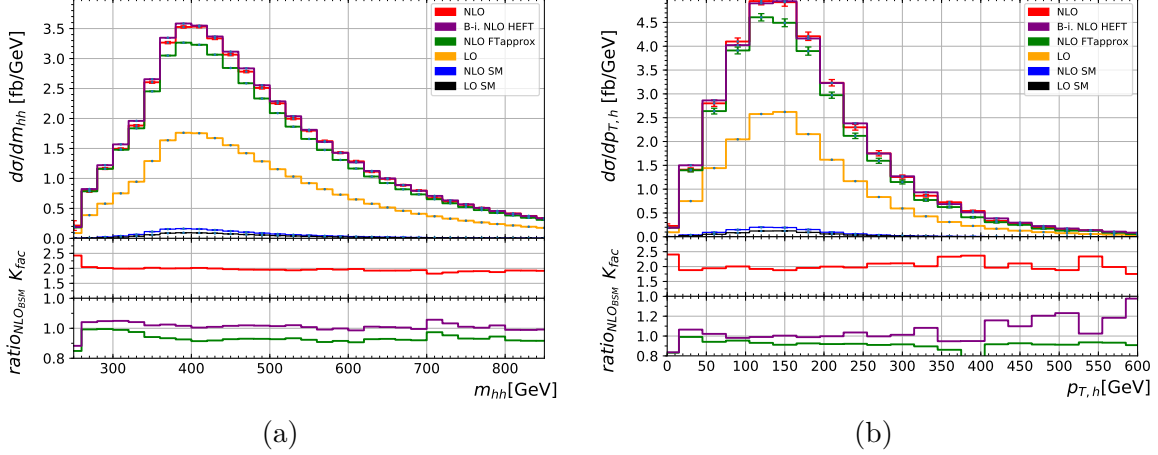


Figure 14: Same as Fig. 12 but for benchmark point 3, $c_{hhh} = 1, c_t = 1, c_{tt} = -1.5, c_{ggh} = 0, c_{gghh} = 4/15$.

Benchmark point 3, shown in Fig. 14, has the same values for c_{hhh} and c_t as benchmark point 2 (the SM values), but the distributions show a very different behaviour. As in the SM, there is a peak around the $2m_t$ threshold, but the cross section is largely enhanced, not only in the peak region. As mentioned above, with a total cross section of about 32 times the SM NLO cross section, this parameter point is above the current limit deduced at 95% CL from the measured $pp \rightarrow HH \rightarrow \gamma\gamma b\bar{b}$ cross section [97, 98]. Benchmark point 4, shown in Fig. 15, has negative values for c_{hhh} and c_{tt} , a slightly increased Yukawa coupling c_t , and no Higgs-gluon contact interactions. This combination removes the destructive interference between different types of diagrams present in the SM, and therefore leads to a very large cross section. The differential K-factor is about 2, as for the other benchmarks, and rather constant over the whole m_{hh} range (whereas for benchmark 2, the differential K-factor is far from being homogeneous). Benchmark 4 is the one with the largest cross section of all the considered benchmark points, with a total cross section of about 270 times the SM one. This point in parameter space is excluded already. Therefore, in Fig. 16, we also show results for another point from cluster 4, defined by $c_{hhh} = 1, c_t = 1, c_{tt} = 0, c_{ggh} = 4/15, c_{gghh} = -0.2$, which leads to a similar shape as benchmark point 4, but to $\sigma/\sigma_{SM} = 1.8$, and hence is not yet

excluded. This parameter point also has the interesting feature that the distributions for NLO SM and LO BSM almost coincide. However, there is no degeneracy with the SM distribution once the NLO corrections are taken into account.

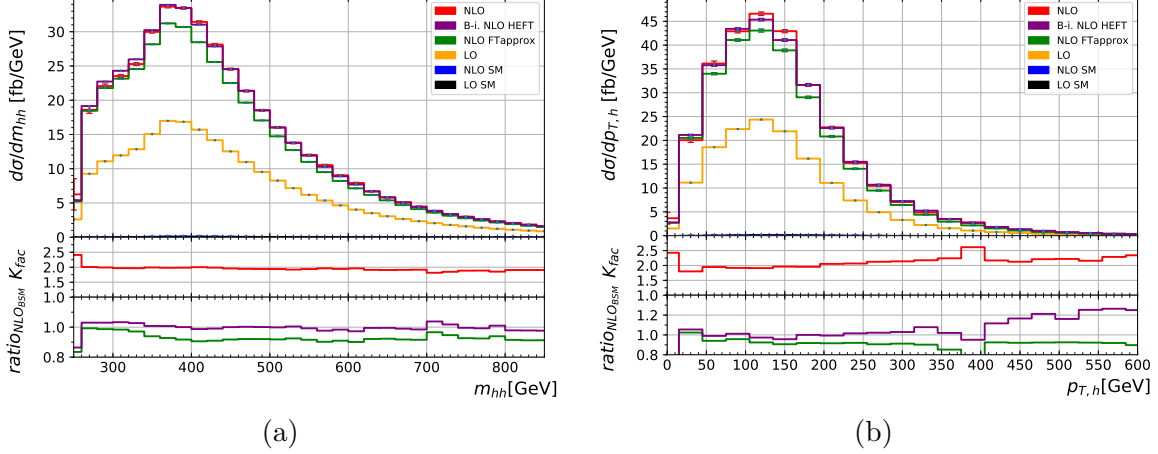


Figure 15: Same as Fig. 12 but for benchmark point 4, $c_{hhh} = -3.5$, $c_t = 1.5$, $c_{tt} = -3$, $c_{ggh} = c_{gghh} = 0$.

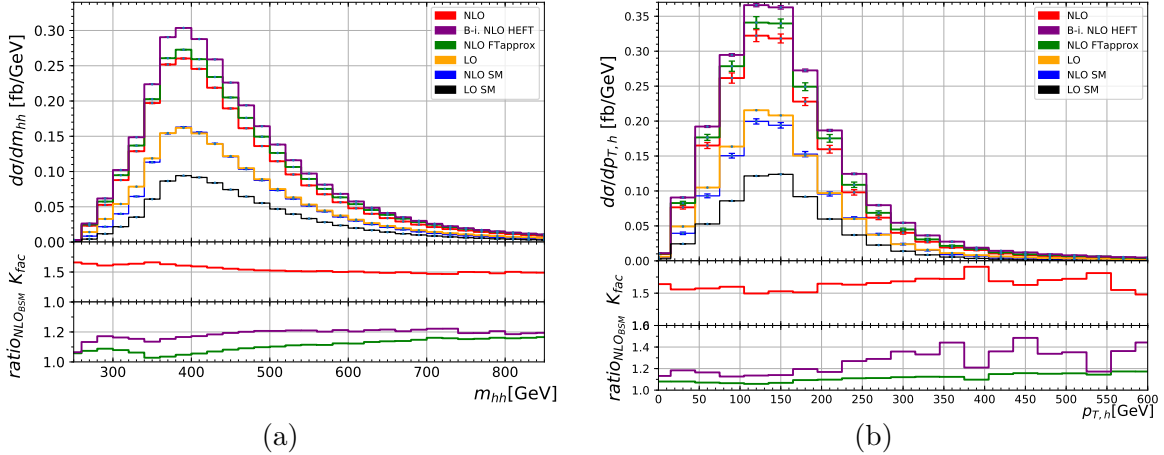


Figure 16: A point from cluster 4, $c_{hhh} = 1$, $c_t = 1$, $c_{tt} = 0$, $c_{ggh} = 4/15$, $c_{gghh} = -0.2$, which leads to a similar shape as benchmark point 4, but to a much smaller cross section.

Fig. 17 shows distributions for benchmark point 5, where c_{tt} is zero and c_{hhh} and c_t are as in the SM, while the Higgs-gluon interactions are nonzero. Similar to benchmark point 2, we observe a dip near $m_{hh} = 350$ GeV, but the LO HEFT amplitude does not

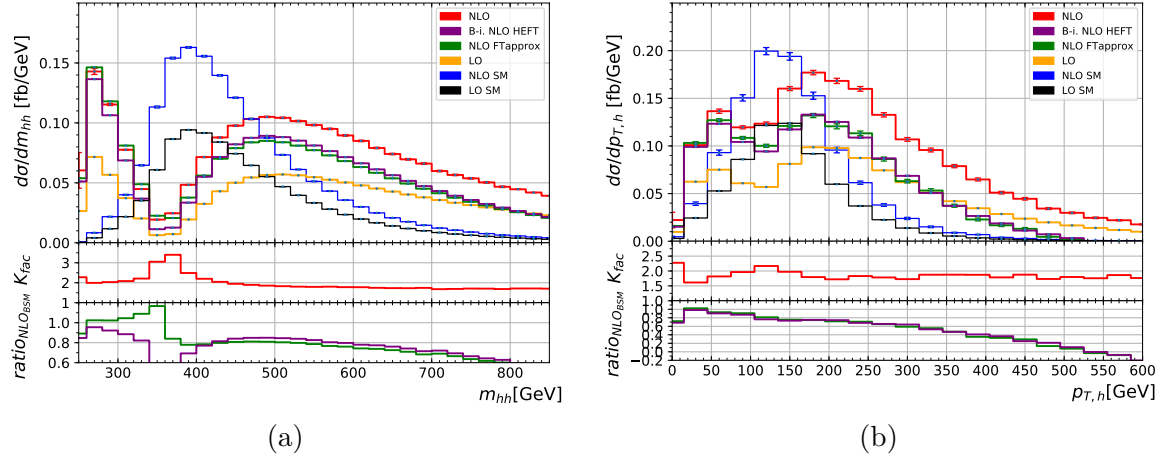


Figure 17: Same as Fig. 12 but for benchmark point 5, $c_{hhh} = 1, c_t = 1, c_{tt} = 0, c_{ggh} = 8/15, c_{gghh} = 1/3$.

vanish there. The total cross section for benchmark point 5 is very similar to the SM one. This is an example where differential measurements are crucial to establish a clear BSM signal. The $p_{T,h}$ distribution shows the rather unexpected behaviour that FT_{approx} and Born-improved HEFT drop very rapidly at large values of $p_{T,h}$. The reason is that the rescaling factor B_{FT}/B_{HEFT} becomes very large as the energy increases, because B_{HEFT} does not grow with \hat{s} for this combination of couplings, but becomes very small. Therefore the negative virtual corrections are multiplied by a very large factor, leading to the fall-off of the green and purple curves in the tail of the $p_{T,h}$ distribution.

Benchmark point 6, shown in Fig. 18, also shows a dip, related to the fact that the LO HEFT amplitude exactly vanishes at $m_{hh} = 429$ GeV. In addition it has a large enhancement of the low m_{hh} region due to the value $c_{hhh} = 2.4$. Note that this value for c_{hhh} is very close to the point where the total cross section as a function of c_{hhh} goes through a minimum if all other couplings are kept SM-like.

Benchmark point 7, shown in Fig. 19, has the same values for c_{ggh}, c_{gghh}, c_t and c_{tt} as benchmark point 6, but a different value for c_{hhh} ($c_{hhh} = 5$). This makes the dip disappear completely, leading to a total cross section which is about 6.7 times larger than the one for benchmark 6, and a large enhancement of the low m_{hh} and low $p_{T,h}$ regions. The distributions also show that the full top quark mass dependence in the “triangle-type” diagrams containing c_{hhh} , which dominate the low m_{hh} region, seems to play a significant role, as the full NLO result is quite different from the approximate results.

Benchmark point 8a, displayed in Fig. 20, again shows a characteristic dip just before

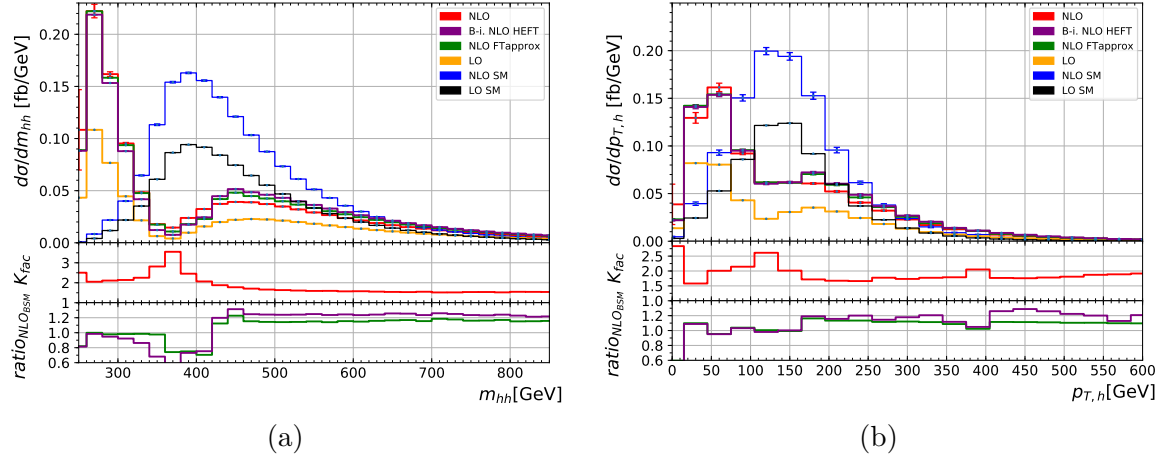


Figure 18: Same as Fig. 12 but for benchmark point 6, $c_{hhh} = 2.4, c_t = 1, c_{tt} = 0, c_{ggh} = 2/15, c_{gghh} = 1/15$.

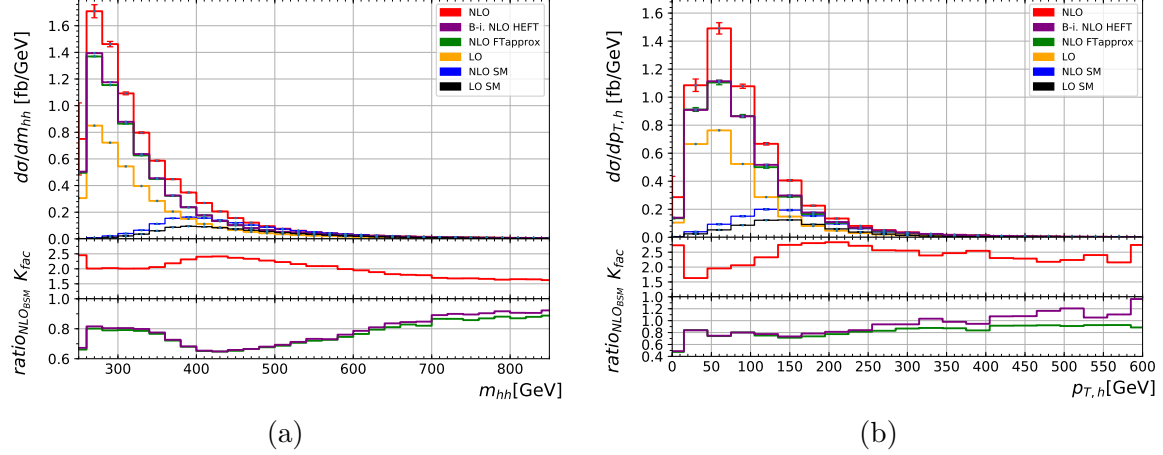


Figure 19: Same as Fig. 12 but for benchmark point 7, $c_{hhh} = 5, c_t = 1, c_{tt} = 0, c_{ggh} = 2/15, c_{gghh} = 1/15$.

the $2m_t$ threshold. It is also an example where the total cross section is very similar to the SM one, but the shape of both the m_{hh} and the $p_{T,h}$ distributions clearly discriminates the SM from the BSM case.

Benchmark point 9, displayed in Fig. 21, shows a large enhancement in the tails of the distributions, similar to benchmarks 2 and 3, which can be attributed mainly to the rather large value of c_{gghh} , in combination with a non-zero value of c_{tt} .

For benchmark point 10, shown in Fig. 22, the large value of $c_{hhh} = 10$ completely dominates the shape, leading to a large enhancement in the low m_{hh} and $p_{T,h}$ regions.

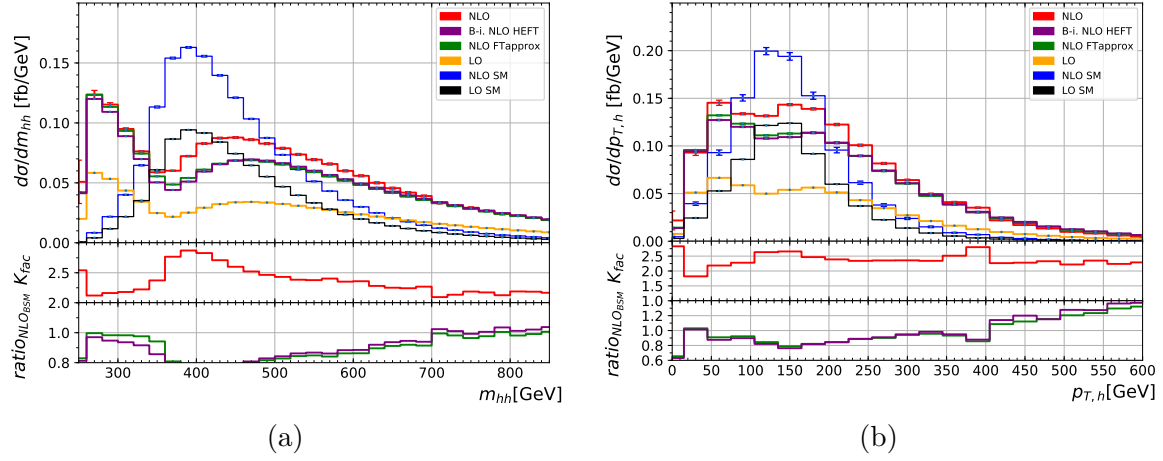


Figure 20: Same as Fig. 12 but for benchmark point 8a, $c_{hhh} = 1, c_t = 1, c_{tt} = 0.5, c_{ggh} = 4/15, c_{gghh} = 0$.

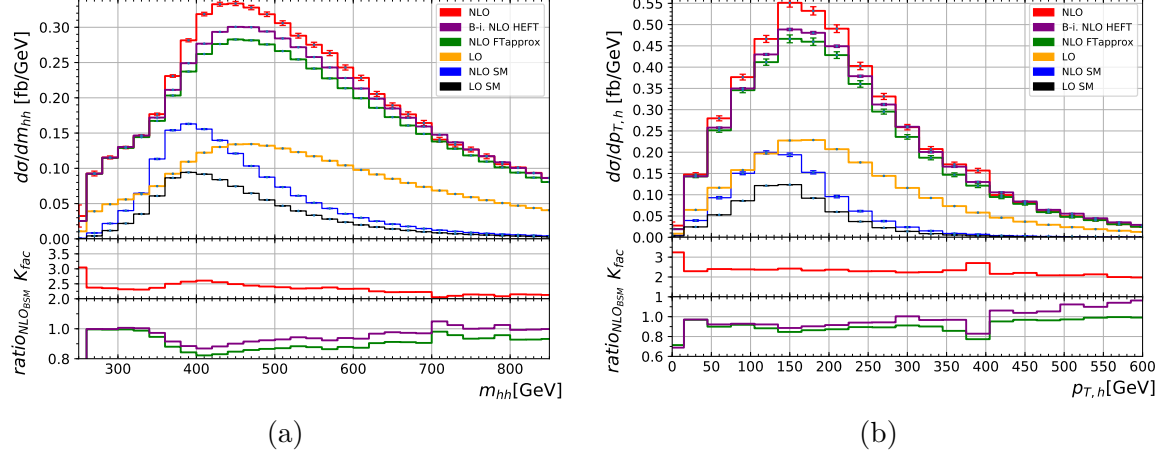


Figure 21: Same as Fig. 12 but for benchmark point 9, $c_{hhh} = 1, c_t = 1, c_{tt} = 1, c_{ggh} = -0.4, c_{gghh} = -0.2$.

With a value for the total cross section which is about 17 times larger than the SM cross section, benchmark point 10 is still allowed by the limits given by CMS [97], where separate limits for the various benchmark points are given.

Benchmark point 11, displayed in Fig. 23, has the same value for c_{hhh} as benchmark 6, which is the one where the destructive interference would be maximal if all other couplings are kept SM-like. However, the destructive interference is compensated by the large and non-zero values of c_{ggh} and c_{gghh} , such that the total cross section for benchmark 11 is about 5 times larger than the SM cross section. In view of the

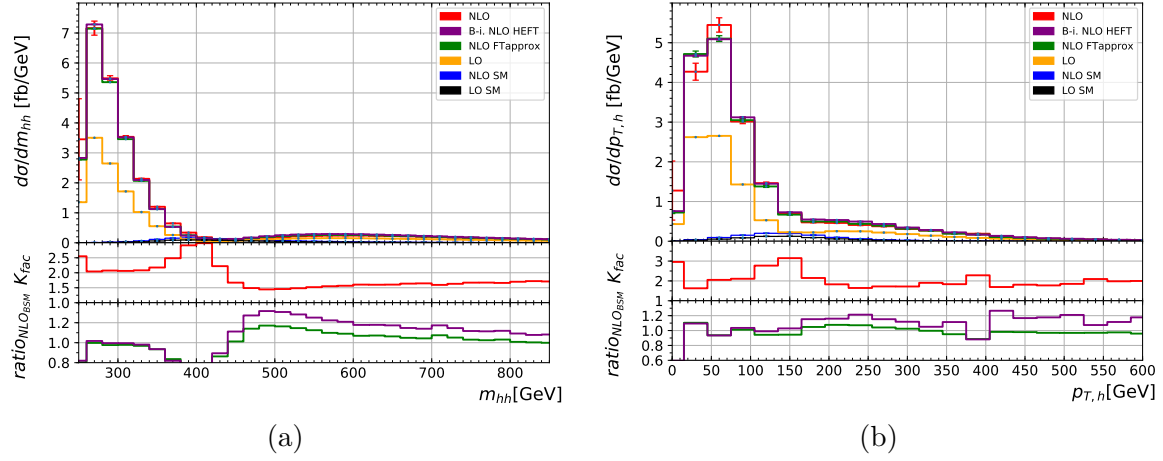


Figure 22: Same as Fig. 12 but for benchmark point 10, $c_{hhh} = 10, c_t = 1.5, c_{tt} = -1, c_{ggh} = c_{gghh} = 0$.

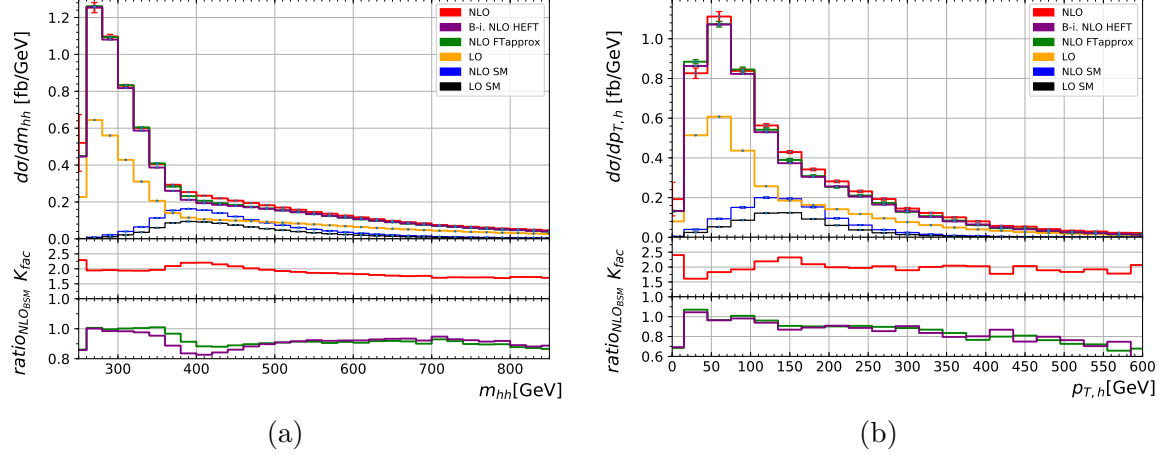


Figure 23: Same as Fig. 12 but for benchmark point 11, $c_{hhh} = 2.4, c_t = 1, c_{tt} = 0, c_{ggh} = 2/3, c_{gghh} = 1/3$.

fact that this benchmark point is dominated by the Higgs-gluon contact interactions parametrised by c_{ggh} and c_{gghh} , it is not a surprise that the approximations $\text{FT}_{\text{approx}}$ and Born-improved HEFT agree quite well with the full calculation, as all three curves have these contributions in common, while the part which differs is damped by the destructive interference.

Benchmark point 12, shown in Fig. 24, has all couplings SM-like except $c_{tt} = 1$ and c_{hhh} , where for the latter an extreme value of $c_{hhh} = 15$ is chosen, leading to a cross section about 100 times larger than the SM cross section. This scenario is already ruled

out by current LHC measurements.

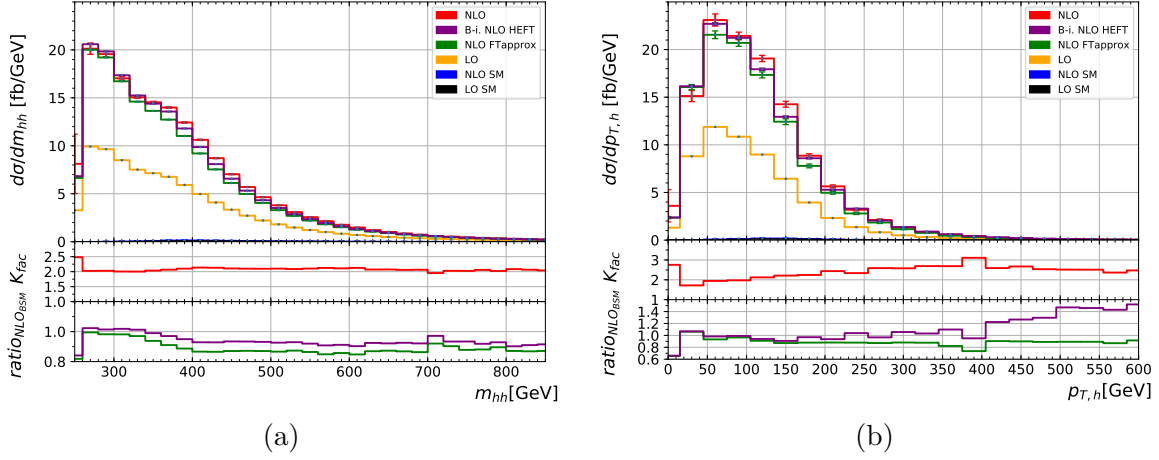


Figure 24: Same as Fig. 12 but for benchmark point 12, $c_{hhh} = 15, c_t = 1, c_{tt} = 1, c_{ggh} = c_{gggh} = 0$.

All the distributions show that the NLO K-factors are large, being about a factor of two or larger. Therefore it is essential to take NLO corrections into account. The approximations where the top quark mass dependence is only partly taken into account also differ substantially in the shape from the full result for some of the benchmark points, which emphasises the importance of including the full top quark mass dependence.

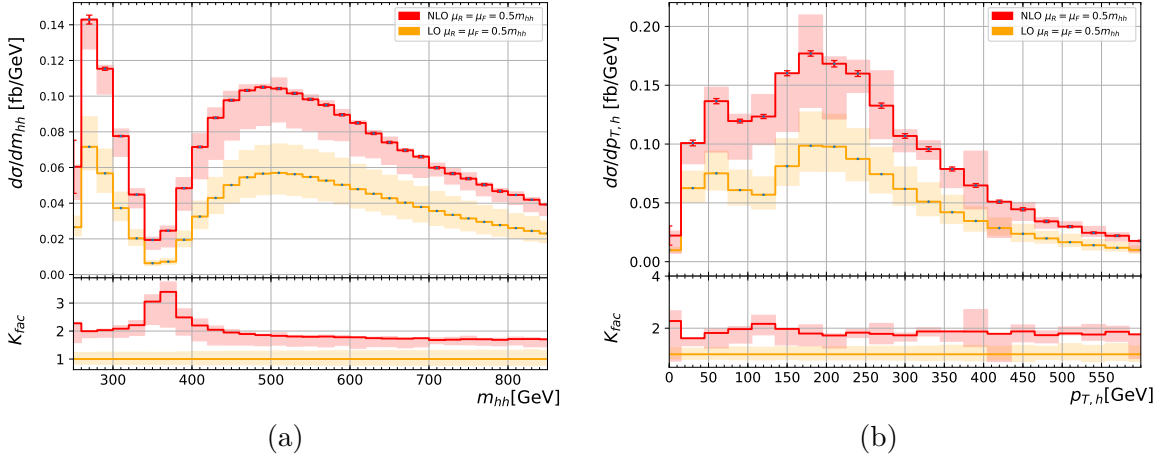


Figure 25: Scale variations for benchmark point 5.

In Fig. 25, we show the LO and NLO scale variation bands for benchmark point 5. This benchmark point is an example where the scale variation band of the 7-point

scale variation mainly decreases the differential cross section over almost the whole m_{hh} range, where the upper limit of the scale variation band is mostly given by the combination $\mu_F = \mu_0/2, \mu_R = \mu_0$, for some of the bins also by $\mu_F = \mu_0, \mu_R = 2\mu_0$. In the SM, the upper limit of the 7-point scale variation band is given by $\mu_F = \mu_R = \mu_0$ for all bins of the m_{hh} distribution. We further notice that LO and NLO scale variation bands do not overlap for the m_{hh} distribution. However, this feature is also present in the SM.

3.2.3 Discussion of the benchmark points

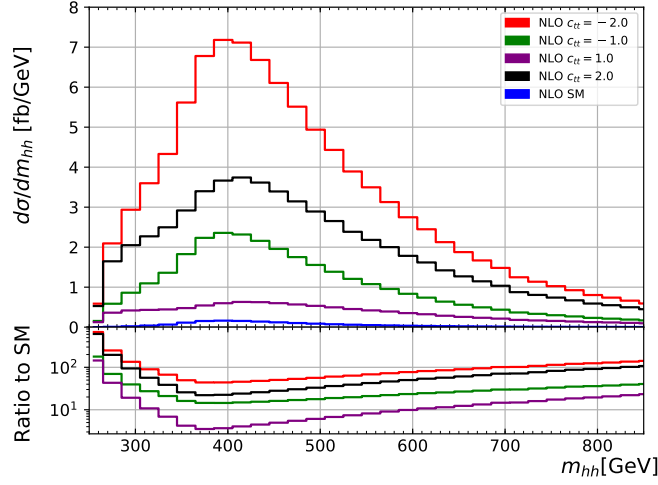


Figure 26: Higgs boson pair invariant mass distributions for various values of c_{tt} .

Attempting a more global view of the behaviour of the m_{hh} distribution as a function of the five BSM parameters, we can identify the following patterns: a dip in the m_{hh} distributions is present for benchmark points 1, 2, 5, 6 and 8a. The presence of a non-zero value for c_{tt} or c_{ggh} is a characteristic feature of many parameter space points that show a dip in the m_{hh} distribution, but this is not a necessary condition for the presence of the dip. For instance, points with $c_{hhh} \simeq 2.5c_t$ and the other couplings vanishing also show such a dip. For the subset (1, 2, 6) of the above points there is a m_{hh} value where the LO amplitude in the $m_t \rightarrow \infty$ limit exactly vanishes, which is a feature that can cause the dip. The low m_{hh} region is enhanced for benchmark points 1, 6, 7, 10, 11, 12, which is mainly due to the large value of c_{hhh} , as the matrix element squared proportional to c_{hhh}^2 for large \hat{s} behaves like $m_h^2/\hat{s} \log^2(m_t^2/\hat{s})$ [31] and therefore dominates at low values of \hat{s} . The term proportional to c_{tt}^2 for large \hat{s} behaves like $\log^2(m_t^2/\hat{s})$ and seems to partially cancel the logarithmic terms from c_{hhh} , such that

benchmark 4 has a SM-like shape even though the absolute value for c_{hhh} is large. The matrix element squared proportional to c_{gghh} grows like \hat{s} , this is why for benchmark points which have large values of c_{gghh} , the tail of the m_{hh} distribution is enhanced. In order to assess the effect of a variation of c_{tt} while the other couplings are fixed to their SM values, we show m_{hh} distributions for the c_{tt} values $c_{tt} = -2, -1, 0, 1, 2$ in Fig. 26. The minimum of the cross section is at $c_{tt} \sim 0.25$. We observe that the enhancement of the cross section as $|c_{tt}|$ increases is growing more rapidly for negative values of c_{tt} , see also Fig. 8b. The shape changes compared to the SM are most pronounced in the low m_{hh} region.

4 Conclusions

We have calculated the NLO QCD corrections with full m_t dependence to Higgs boson pair production within the framework of the electroweak chiral Lagrangian, a non-linearly realised Effective Field Theory in the Higgs sector, which allows to focus on anomalous Higgs boson properties. This restricts the BSM parameter space to five possibly anomalous couplings, c_{hhh} , c_t , c_{tt} , c_{ggh} and c_{gghh} .

We gave a parametrisation of the total NLO cross section and of the m_{hh} distribution in terms of 23 coefficients of all combinations of these couplings, and also showed iso-contours of LO and NLO cross section ratios σ/σ_{SM} for two-dimensional projections of the parameter space. These studies showed that the cross sections are very sensitive to variations of c_{tt} , the effective $t\bar{t}hh$ coupling, and that the K-factors can be large and non-uniform as the anomalous couplings are varied.

We have also shown differential cross sections for m_{hh} and $p_{T,h}$ at several benchmark points which exhibit characteristic shapes of the distributions. The differential K-factors for the m_{hh} distributions are of the order of two, but can reach up to three and can be very non-uniform over the m_{hh} range. This means that a rescaling of the LO distribution with a global K-factor can be rather misleading.

Some combinations of couplings lead to a huge enhancement of the cross section, others lead to a total cross section which is nearly degenerate to the SM one, but the corresponding m_{hh} and $p_{T,h}$ distributions have a shape which is very different from the SM one, and therefore should have discriminating power even with low statistics, which emphasises the importance of measuring distributions.

Our analytical parametrisation of the total NLO cross section and of the m_{hh} distribution in terms of all possible combinations of anomalous couplings should open the door to further studies of the considered BSM parameter space and lead to refined limits on anomalous Higgs boson couplings in the not too distant future.

Acknowledgements

We would like to thank Luca Cadamuro, Oscar Cata, Nicolas Greiner, Ramona Gröber, Stephen Jones, Matthias Kerner, Gionata Luisoni, Joao Pires and Johannes Schlenk for many helpful discussions. We also thank Alexandra Carvalho and Florian Goertz for useful communication. This research was supported in part by the COST Action CA16201 (‘Particleface’) of the European Union and by the DFG cluster of excellence EXC 153 ‘Origin and Structure of the Universe’ and DFG grant BU 1391/2-1. We gratefully acknowledge resources provided by the Max Planck Computing and Data Facility (MPCDF).

A Appendix

A.1 Differential coefficients of all coupling combinations for m_{hh}

In order to allow a flexible use of our results, we provide tables for the differential coefficients of the various coupling combinations contributing to the m_{hh} distribution. They are given in `.csv` format as ancillary files to the arXiv submission and the JHEP publication. The conventions are as follows. The given numbers are the coefficients \tilde{A}_i of the coupling combinations c_i as given in eq. (3.1). We call them \tilde{A}_i rather than A_i to make clear that they are the *differential* coefficients. In more detail, we provide the coefficients \tilde{A}_i in

$$\frac{d\sigma}{dm_{hh}} = \sum_{i=1}^{23} \tilde{A}_i c_i \quad (\text{A.1})$$

in units of fb/GeV, where the c_i stand for the 23 possible combinations of couplings, in the same order as in Eq. (3.1). We should point out that the \tilde{A}_i are *not* normalised by the SM values. The numbers in the 24 columns are m_{hh} (bin center), $\tilde{A}_1, \dots, \tilde{A}_{23}$. Each line gives the numbers for one bin in m_{hh} , with a bin size of 20 GeV. We give results for 40 bins, corresponding to the range $250 \text{ GeV} \leq m_{hh} \leq 1030 \text{ GeV}$ (bin center values).

The coefficients have been determined by evaluating 23 differential cross sections, obtained by changing the values of the five coupling parameters. Then the system of 23 equations is solved to extract the value of each coefficient \tilde{A}_i .

A.2 Relation between EWChL and SMEFT

Accounting for deviations from the SM within a low-energy, bottom-up effective field theory requires a power-counting prescription. The power counting determines, in a systematic manner, which corrections to include, and which ones to neglect, under certain

assumptions that need to be specified. The power counting of the Higgs-electroweak chiral Lagrangian has been reviewed in Sec. 2.1. In this appendix we discuss how the analysis of $gg \rightarrow hh$ within the EWChL is related to a treatment of this process using SMEFT.

SMEFT is an EFT at the weak scale v , organised primarily by the canonical dimension of operators. This corresponds to the assumption that New Physics enters at some generic scale Λ , presumably in the TeV range, and is weakly coupled to the SM fields. The renormalisable SM then represents the leading-order term. The leading corrections are given by operators of canonical dimension 6 (apart from a single, lepton-number violating operator of dimension 5, which is not relevant in the present context) [3, 4]. The dimension-6 terms relevant for $gg \rightarrow hh$ can be written as

$$\begin{aligned} \Delta\mathcal{L}_6 = & \frac{\bar{c}_H}{2v^2} \partial_\mu(\phi^\dagger\phi) \partial^\mu(\phi^\dagger\phi) + \frac{\bar{c}_u}{v^2} y_t(\phi^\dagger\phi \bar{q}_L \tilde{\phi} t_R + \text{h.c.}) - \frac{\bar{c}_6}{2v^2} \frac{m_h^2}{v^2} (\phi^\dagger\phi)^3 \\ & + \frac{\bar{c}_{ug}}{v^2} g_s(\bar{q}_L \sigma^{\mu\nu} G_{\mu\nu} \tilde{\phi} t_R + \text{h.c.}) + \frac{4\bar{c}_g}{v^2} g_s^2 \phi^\dagger\phi G_{\mu\nu}^a G^{a\mu\nu} . \end{aligned} \quad (\text{A.2})$$

Here we follow the conventions used in [68], except for \bar{c}_g , which includes an extra factor of the electroweak coupling g^2 in the definition of [68]. We are assuming CP conservation to leading order in $\Delta\mathcal{L}_6$. Then all coefficients in (A.2) are real and the CP-odd operator $\phi^\dagger\phi \tilde{G}_{\mu\nu}^a G^{a\mu\nu}$ can be omitted.

The SM amplitude for $gg \rightarrow hh$ (first and third diagram in the top row of Fig. 1) arises at one-loop order, counting as $A_{SM} = \mathcal{O}(1/16\pi^2)$. Considering the next order in SMEFT based on (A.2), we may distinguish two cases.

- i) Pure dimensional counting: In this case we only assume that the dimension-6 operators in the SMEFT Lagrangian are suppressed by a factor of $1/\Lambda^2$ from dimensional analysis. The coefficients in (A.2) are thus treated as $\bar{c}_i = \mathcal{O}(v^2/\Lambda^2)$ by power counting. It then follows that the dominant correction comes from the operator $\phi^\dagger\phi G_{\mu\nu}^a G^{a\mu\nu}$ through the tree diagrams in the bottom row of Fig. 1. This correction to the amplitude counts as $\Delta A_g = \mathcal{O}(v^2/\Lambda^2)$, a suppression that is competing with the loop factor of A_{SM} . All other operators in (A.2) correct vertices within the SM loop diagrams and therefore contribute $\Delta A_{\text{other}} = \mathcal{O}((1/16\pi^2)(v^2/\Lambda^2))$. This is a subleading effect, negligible in the scenario under consideration. The dominant correction is thus described by a single parameter, \bar{c}_g . In view of typical New-Physics models, such a scenario appears unrealistic. To generalise the treatment, dimensional counting needs to be supplemented by further assumptions, as discussed in the next item.
- ii) Dimensional counting including loop factors: Supposing that the New Physics at scale Λ is a weakly coupled gauge theory, it can be shown that dimension-6

operators with field-strength factors are only generated through loop diagrams [4, 101]. Their coefficients then come with an extra factor of $1/16\pi^2$. In this case, the coefficients \bar{c}_{ug} and \bar{c}_g in (A.2) are counted as order $(1/16\pi^2)(v^2/\Lambda^2)$, while \bar{c}_H , \bar{c}_u and \bar{c}_6 are still of order v^2/Λ^2 . As a consequence, the leading-order corrections to the SM amplitude for $gg \rightarrow hh$ (see Fig. 1) come from the tree-diagrams with \bar{c}_g , as well as from top-loop diagrams with vertices modified by \bar{c}_H , \bar{c}_u and \bar{c}_6 . All these corrections count as order $(1/16\pi^2)(v^2/\Lambda^2)$, a relative correction of order v^2/Λ^2 to A_{SM} .

This discussion of applying SMEFT to $gg \rightarrow hh$ has several implications:

- a) Note that under both scenarios i) and ii) the magnetic-moment type operator $\bar{q}_L \sigma^{\mu\nu} G_{\mu\nu} \tilde{\phi} t_R$ gives only a subleading contribution (of order $1/16\pi^2$ times the leading correction) and can be consistently neglected.
- b) We emphasise that the loop suppression of operators with field-strength factors in scenario ii) follows the rules of chiral counting. The Higgs-gluon operator, for example, is given by $\kappa^2 \phi^\dagger \phi g_s^2 G_{\mu\nu}^a G^{a\mu\nu}$, when we include the weak⁴ couplings, g_s for each gluon, and κ for the coupling of ϕ to the heavy sector. The chiral dimension of the Higgs-gluon operator is then $d_\chi \equiv 2L+2 = 6$, corresponding to a loop order of $L = 2$. Taking into account the canonical dimension, the coefficient is estimated as [102]

$$\frac{1}{v^2} \frac{1}{(16\pi^2)^2} = \frac{1}{\Lambda^2} \frac{1}{16\pi^2} , \quad (\text{A.3})$$

where we used the NDA relation $\Lambda = 4\pi v$ [103]. This implies a \bar{c}_g of order $(1/16\pi^2)(v^2/\Lambda^2)$, in agreement with [101]. A similar argument holds for \bar{c}_{ug} .

- c) The coefficients \bar{c}_i may be related to the couplings of the physical Higgs field h and compared with the corresponding parameters of the chiral Lagrangian (2.6). After a field redefinition of h to eliminate \bar{c}_H from the kinetic term one finds [31, 68]

$$c_t = 1 - \frac{\bar{c}_H}{2} - \bar{c}_u , \quad c_{tt} = -\frac{\bar{c}_H + 3\bar{c}_u}{2} , \quad c_{hhh} = 1 - \frac{3}{2}\bar{c}_H + \bar{c}_6 , \quad (\text{A.4})$$

$$c_{ggh} = 2c_{gghh} = 128\pi^2 \bar{c}_g . \quad (\text{A.5})$$

- d) After taking into account factors from loop counting in scenario ii), the parametrisation of New-Physics effects in $gg \rightarrow hh$ is similar in SMEFT and in the EWChL,

⁴In the context of power counting, “weak coupling” means a coupling of order unity, as opposed to a strong coupling of order 4π .

as is apparent from (A.4) and (A.5). However, there are still notable differences. While the four SMEFT coefficients \bar{c}_H , \bar{c}_u , \bar{c}_6 and $16\pi^2 \bar{c}_g$ are parametrically small, of order v^2/Λ^2 , the non-linear coefficients c_t , c_{tt} , c_{hhh} , c_{ggh} and c_{gghh} may be treated as quantities of order one. No further expansion in the latter coefficients is needed when computing cross sections, whereas the SMEFT coefficients should only be kept to first order when working at the level of dimension-6 operators. It appears that the SMEFT treatment has only 4 parameters, instead of 5 for the EWChL, due to the relation in (A.5). It should, however, be kept in mind that the extraction of Higgs couplings ultimately requires a global analysis, where other Higgs-related processes are also taken into account. In this case, in particular for the important single-Higgs observables, the EWChL has overall fewer parameters to describe leading NP effects [76]. It has the advantage to focus on anomalous Higgs properties and to naturally allow for large deviations from the SM in the Higgs sector.

B Erratum

After comparison with the authors of Ref. [104], it turned out that the two-loop amplitude used in the original version of this work was missing a term related to triangle-type diagrams, affecting the cases where the ratio between trilinear Higgs coupling c_{hhh} and Yukawa coupling modifier c_t is different from 1 (i.e. the Standard Model (SM) value), or when the effective coupling of a $t\bar{t}$ pair to a Higgs pair, c_{tt} , is nonzero. The SM results are unchanged. Therefore, benchmark points with a value of c_{hhh}/c_t or c_{tt} very different from the SM are the most affected. We have recalculated the values for the cross sections at the 12 benchmark points shown in Table 3 of the main text. In Table 5, we show a comparison of the corrected values for the cross sections to the previous values.

In Fig. 27 we show the effects of the correction on the m_{hh} distribution for benchmark points 1 and 10, which are affected most due to their large value of c_{hhh} . The differences are found to be below $\sim 20\%$ and therefore within the scale and top mass scheme uncertainties. In general, we have observed that the relative size of the scale uncertainty bands is not significantly affected by the correction.

Benchmark	$\sigma_{\text{NLO}}^{\text{old}}$ [fb]	$\sigma_{\text{NLO}}^{\text{new}}$ [fb]			$\sigma_{\text{NLO}}^{\text{new}}/\sigma_{\text{NLO,SM}}$
	14 TeV	13 TeV	13.6 TeV	14 TeV	14 TeV
B_1	194.89	150.80	168.35	180.53	5.48
B_2	14.55	10.06	11.51	12.54	0.38
B_3	1047.37	803.78	894.69	957.79	29.07
B_4	8922.75	7050.62	7811.76	8338.07	253.05
B_5	59.325	48.66	54.93	59.33	1.80
B_6	24.69	20.73	22.97	24.53	0.74
B_7	169.41	140.97	154.92	164.52	4.99
B_{8a}	41.70	30.36	33.87	36.32	1.10
B_9	146.00	101.63	114.01	122.66	3.72
B_{10}	575.86	481.17	529.65	563.00	17.09
B_{11}	174.70	145.84	161.91	173.06	5.25
B_{12}	3618.53	2925.69	3223.98	3429.40	104.08

Table 5: Comparison of the total cross section values at NLO before and after the correction at a centre-of-mass energy of $\sqrt{s} = 14$ TeV and ratio of the new values to the SM cross section, $\sigma_{\text{NLO,SM}}(14 \text{ TeV}) = 32.95 \text{ fb}$. In addition, we provide corrected cross-section values at $\sqrt{s} = 13$ TeV and 13.6 TeV.

We also provide a new fit of the A_i coefficients at NLO,

$$\begin{aligned}
\frac{\sigma_{\text{NLO}}}{\sigma_{\text{NLO,SM}}} = & A_1 c_t^4 + A_2 c_{tt}^2 + A_3 c_t^2 c_{hhh}^2 + A_4 c_{ggh}^2 c_{hhh}^2 + A_5 c_{gghh}^2 + A_6 c_{tt} c_t^2 + A_7 c_t^3 c_{hhh} \\
& + A_8 c_{tt} c_t c_{hhh} + A_9 c_{tt} c_{ggh} c_{hhh} + A_{10} c_{tt} c_{gghh} + A_{11} c_t^2 c_{ggh} c_{hhh} + A_{12} c_t^2 c_{gghh} \\
& + A_{13} c_t c_{hhh}^2 c_{ggh} + A_{14} c_t c_{hhh} c_{gghh} + A_{15} c_{ggh} c_{hhh} c_{gghh} \\
& + A_{16} c_t^3 c_{ggh} + A_{17} c_t c_{tt} c_{ggh} + A_{18} c_t c_{ggh}^2 c_{hhh} + A_{19} c_t c_{ggh} c_{gghh} \\
& + A_{20} c_t^2 c_{ggh}^2 + A_{21} c_{tt} c_{ggh}^2 + A_{22} c_{ggh}^3 c_{hhh} + A_{23} c_{ggh}^2 c_{gghh} ,
\end{aligned} \tag{A.1}$$

as given in Table 1. For the corrected values, our treatment of the uncertainties has also improved, now including statistical uncertainties from the sample of BSM points as well as correlations among the coefficients. We provide them in Table 6 for $\sqrt{s} = 13$ and 13.6 TeV, with $\sigma_{\text{NLO,SM}}(13 \text{ TeV}) = 27.80 \text{ fb}$ and $\sigma_{\text{NLO,SM}}(13.6 \text{ TeV}) = 30.82 \text{ fb}$.

We also updated the ancillary files available on arXiv for the A_i coefficients, both for the inclusive cross sections and the cross sections differential in m_{HH} , at $\sqrt{s} = 13$ TeV

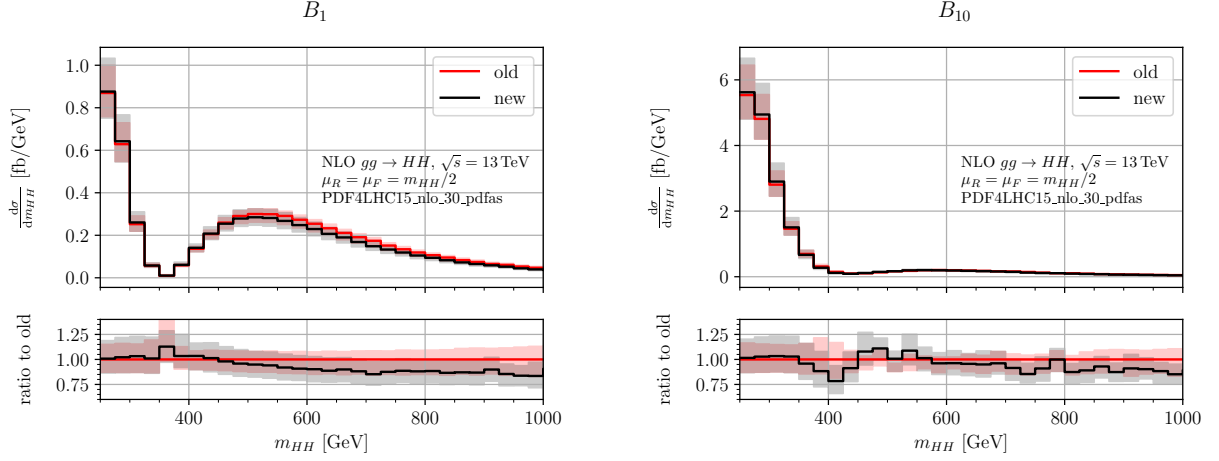


Figure 27: Comparison of old and new results for the cross sections differential in m_{hh} for benchmark points 1 and 10 of Table 3 in the main text, at $\sqrt{s} = 13$ TeV.

and $\sqrt{s} = 13.6$ TeV.

We would like to thank the authors of Ref. [104] for pointing us to the discrepancy with their result.

References

- [1] **ATLAS, CMS** Collaboration, G. Aad et al., *Measurements of the Higgs boson production and decay rates and constraints on its couplings from a combined ATLAS and CMS analysis of the LHC pp collision data at $\sqrt{s} = 7$ and 8 TeV*, *JHEP* **08** (2016) 045, [[arXiv:1606.02266](#)].
- [2] G. Brooijmans et al., *Les Houches 2017: Physics at TeV Colliders New Physics Working Group Report*, in *10th Les Houches Workshop on Physics at TeV Colliders (PhysTeV 2017) Les Houches, France, June 5-23, 2017*, 2018. [[arXiv:1803.10379](#)].
- [3] W. Buchmüller and D. Wyler, *Effective Lagrangian Analysis of New Interactions and Flavor Conservation*, *Nucl. Phys.* **B268** (1986) 621–653.
- [4] B. Grzadkowski, M. Iskrzynski, M. Misiak, and J. Rosiek, *Dimension-Six Terms in the Standard Model Lagrangian*, *JHEP* **10** (2010) 085, [[arXiv:1008.4884](#)].
- [5] L. Berthier and M. Trott, *Towards consistent Electroweak Precision Data constraints in the SMEFT*, *JHEP* **05** (2015) 024, [[arXiv:1502.02570](#)].
- [6] M. Ghezzi, R. Gomez-Ambrosio, G. Passarino, and S. Uccirati, *NLO Higgs effective field theory and κ -framework*, *JHEP* **07** (2015) 175, [[arXiv:1505.03706](#)].

Coefficient	13 TeV	13.6 TeV
A_1	2.20913 ± 0.00034	2.20259 ± 0.00014
A_2	11.2754 ± 0.0041	11.31544 ± 0.00062
A_3	0.334152 ± 0.000073	0.331430 ± 0.000029
A_4	0.3520 ± 0.0011	0.34943 ± 0.00030
A_5	12.631 ± 0.036	12.83225 ± 0.00066
A_6	-9.1965 ± 0.0046	-9.18628 ± 0.00060
A_7	-1.54327 ± 0.00035	-1.53405 ± 0.00014
A_8	3.26347 ± 0.00076	3.25036 ± 0.00023
A_9	2.811 ± 0.011	2.7974 ± 0.0014
A_{10}	16.139 ± 0.025	16.12925 ± 0.00096
A_{11}	-1.2628 ± 0.0077	-1.2534 ± 0.0011
A_{12}	-5.818 ± 0.016	-5.7712 ± 0.0012
A_{13}	0.6485 ± 0.0015	0.64328 ± 0.00021
A_{14}	2.8127 ± 0.0025	2.79661 ± 0.00042
A_{15}	3.1813 ± 0.0098	3.16880 ± 0.00089
A_{16}	-0.0075 ± 0.0052	-0.00877 ± 0.00084
A_{17}	0.023 ± 0.012	0.0219 ± 0.0017
A_{18}	0.0171 ± 0.0034	0.01792 ± 0.00037
A_{19}	0.023 ± 0.030	0.0271 ± 0.0014
A_{20}	-0.0279 ± 0.0011	-0.02741 ± 0.00017
A_{21}	0.079 ± 0.027	0.07335 ± 0.00064
A_{22}	0.0150 ± 0.0033	0.01547 ± 0.00043
A_{23}	0.117 ± 0.036	0.11712 ± 0.00082

Table 6: Updated values of the A_i coefficients at NLO, as per Eq. (A.1). The uncertainties quoted here are statistical and include correlations between coefficients.

[7] J. de Blas, M. Ciuchini, E. Franco, S. Mishima, M. Pierini, L. Reina, and L. Silvestrini, *The Global Electroweak and Higgs Fits in the LHC era, PoS EPS-HEP2017* (2017) 467, [[arXiv:1710.05402](https://arxiv.org/abs/1710.05402)].

[8] I. Brivio and M. Trott, *Scheming in the SMEFT... and a reparameterization*

- invariance!*, *JHEP* **07** (2017) 148, [[arXiv:1701.06424](#)].
- [9] J. Ellis, C. W. Murphy, V. Sanz, and T. You, *Updated Global SMEFT Fit to Higgs, Diboson and Electroweak Data*, [arXiv:1803.03252](#).
 - [10] F. Feruglio, *The Chiral approach to the electroweak interactions*, *Int. J. Mod. Phys. A* **8** (1993) 4937–4972, [[hep-ph/9301281](#)].
 - [11] J. Bagger, V. D. Barger, K.-m. Cheung, J. F. Gunion, T. Han, G. A. Ladinsky, R. Rosenfeld, and C. P. Yuan, *The Strongly interacting $W W$ system: Gold plated modes*, *Phys. Rev. D* **49** (1994) 1246–1264, [[hep-ph/9306256](#)].
 - [12] V. Koulovassilopoulos and R. S. Chivukula, *The Phenomenology of a nonstandard Higgs boson in $W(L) W(L)$ scattering*, *Phys. Rev. D* **50** (1994) 3218–3234, [[hep-ph/9312317](#)].
 - [13] C. P. Burgess, J. Matias, and M. Pospelov, *A Higgs or not a Higgs? What to do if you discover a new scalar particle*, *Int. J. Mod. Phys. A* **17** (2002) 1841–1918, [[hep-ph/9912459](#)].
 - [14] L.-M. Wang and Q. Wang, *Electroweak chiral Lagrangian for neutral Higgs boson*, *Chin. Phys. Lett.* **25** (2008) 1984, [[hep-ph/0605104](#)].
 - [15] B. Grinstein and M. Trott, *A Higgs-Higgs bound state due to new physics at a TeV*, *Phys. Rev. D* **76** (2007) 073002, [[arXiv:0704.1505](#)].
 - [16] R. Contino, C. Grojean, M. Moretti, F. Piccinini, and R. Rattazzi, *Strong Double Higgs Production at the LHC*, *JHEP* **05** (2010) 089, [[arXiv:1002.1011](#)].
 - [17] R. Contino, *The Higgs as a Composite Nambu-Goldstone Boson*, in *Physics of the large and the small, TASI 09, proceedings of the Theoretical Advanced Study Institute in Elementary Particle Physics, Boulder, Colorado, USA, 1-26 June 2009*, pp. 235–306, 2011. [arXiv:1005.4269](#).
 - [18] R. Alonso, M. B. Gavela, L. Merlo, S. Rigolin, and J. Yepes, *The Effective Chiral Lagrangian for a Light Dynamical "Higgs Particle"*, *Phys. Lett. B* **722** (2013) 330–335, [[arXiv:1212.3305](#)]. [Erratum: *Phys. Lett. B* 726, 926 (2013)].
 - [19] G. Buchalla, O. Cata, and C. Krause, *Complete Electroweak Chiral Lagrangian with a Light Higgs at NLO*, *Nucl. Phys. B* **880** (2014) 552–573, [[arXiv:1307.5017](#)]. [Erratum: *Nucl. Phys. B* 913, 475 (2016)].
 - [20] R. L. Delgado, A. Dobado, and F. J. Llanes-Estrada, *One-loop $W_L W_L$ and $Z_L Z_L$ scattering from the electroweak Chiral Lagrangian with a light Higgs-like scalar*, *JHEP* **02** (2014) 121, [[arXiv:1311.5993](#)].
 - [21] G. Buchalla, O. Cata, and C. Krause, *On the Power Counting in Effective Field Theories*, *Phys. Lett. B* **731** (2014) 80–86, [[arXiv:1312.5624](#)].

- [22] G. Buchalla, O. Cata, A. Celis, and C. Krause, *Fitting Higgs Data with Nonlinear Effective Theory*, *Eur. Phys. J.* **C76** (2016), no. 5 233, [[arXiv:1511.00988](#)].
- [23] J. de Blas, O. Eberhardt, and C. Krause, *Current and future constraints on Higgs couplings in the nonlinear Effective Theory*, [arXiv:1803.00939](#).
- [24] A. Pierce, J. Thaler, and L.-T. Wang, *Disentangling Dimension Six Operators through Di-Higgs Boson Production*, *JHEP* **05** (2007) 070, [[hep-ph/0609049](#)].
- [25] R. Contino, M. Ghezzi, M. Moretti, G. Panico, F. Piccinini, and A. Wulzer, *Anomalous Couplings in Double Higgs Production*, *JHEP* **08** (2012) 154, [[arXiv:1205.5444](#)].
- [26] J. Baglio, A. Djouadi, R. Gröber, M. M. Mühlleitner, J. Quevillon, and M. Spira, *The measurement of the Higgs self-coupling at the LHC: theoretical status*, *JHEP* **04** (2013) 151, [[arXiv:1212.5581](#)].
- [27] S. Dawson, E. Furlan, and I. Lewis, *Unravelling an extended quark sector through multiple Higgs production?*, *Phys. Rev.* **D87** (2013), no. 1 014007, [[arXiv:1210.6663](#)].
- [28] M. J. Dolan, C. Englert, and M. Spannowsky, *Higgs self-coupling measurements at the LHC*, *JHEP* **10** (2012) 112, [[arXiv:1206.5001](#)].
- [29] F. Goertz, A. Papaefstathiou, L. L. Yang, and J. Zurita, *Higgs boson pair production in the $D=6$ extension of the SM*, *JHEP* **04** (2015) 167, [[arXiv:1410.3471](#)].
- [30] A. J. Barr, M. J. Dolan, C. Englert, D. E. Ferreira de Lima, and M. Spannowsky, *Higgs Self-Coupling Measurements at a 100 TeV Hadron Collider*, *JHEP* **02** (2015) 016, [[arXiv:1412.7154](#)].
- [31] A. Azatov, R. Contino, G. Panico, and M. Son, *Effective field theory analysis of double Higgs boson production via gluon fusion*, *Phys. Rev.* **D92** (2015), no. 3 035001, [[arXiv:1502.00539](#)].
- [32] M. J. Dolan, C. Englert, N. Greiner, K. Nordstrom, and M. Spannowsky, *$hhjj$ production at the LHC*, *Eur. Phys. J.* **C75** (2015), no. 8 387, [[arXiv:1506.08008](#)].
- [33] J. K. Behr, D. Bortoletto, J. A. Frost, N. P. Hartland, C. Issever, and J. Rojo, *Boosting Higgs pair production in the $b\bar{b}b\bar{b}$ final state with multivariate techniques*, *Eur. Phys. J.* **C76** (2016), no. 7 386, [[arXiv:1512.08928](#)].
- [34] F. Maltoni, E. Vryonidou, and C. Zhang, *Higgs production in association with a top-antitop pair in the Standard Model Effective Field Theory at NLO in QCD*, *JHEP* **10** (2016) 123, [[arXiv:1607.05330](#)].
- [35] F. Kling, T. Plehn, and P. Schichtel, *Maximizing the significance in Higgs boson pair analyses*, *Phys. Rev.* **D95** (2017), no. 3 035026, [[arXiv:1607.07441](#)].
- [36] Q.-H. Cao, G. Li, B. Yan, D.-M. Zhang, and H. Zhang, *Double Higgs production at*

- the 14 TeV LHC and a 100 TeV pp collider, *Phys. Rev.* **D96** (2017), no. 9 095031, [[arXiv:1611.09336](#)].
- [37] S. Di Vita, C. Grojean, G. Panico, M. Riembau, and T. Vantalon, *A global view on the Higgs self-coupling*, *JHEP* **09** (2017) 069, [[arXiv:1704.01953](#)].
- [38] L. Di Luzio, R. Gröber, and M. Spannowsky, *Maxi-sizing the trilinear Higgs self-coupling: how large could it be?*, *Eur. Phys. J.* **C77** (2017), no. 11 788, [[arXiv:1704.02311](#)].
- [39] T. Corbett, A. Joglekar, H.-L. Li, and J.-H. Yu, *Exploring Extended Scalar Sectors with Di-Higgs Signals: A Higgs EFT Perspective*, *JHEP* **05** (2018) 061, [[arXiv:1705.02551](#)].
- [40] S. Dawson and C. W. Murphy, *Standard Model EFT and Extended Scalar Sectors*, *Phys. Rev.* **D96** (2017), no. 1 015041, [[arXiv:1704.07851](#)].
- [41] A. Alves, T. Ghosh, and K. Sinha, *Can We Discover Double Higgs Production at the LHC?*, *Phys. Rev.* **D96** (2017), no. 3 035022, [[arXiv:1704.07395](#)].
- [42] A. Adhikary, S. Banerjee, R. K. Barman, B. Bhattacharjee, and S. Niyogi, *Revisiting the non-resonant Higgs pair production at the HL-LHC*, *Physics* **2018** (2018) 116, [[arXiv:1712.05346](#)].
- [43] J. H. Kim, Y. Sakaki, and M. Son, *Combined analysis of double Higgs production via gluon fusion at the HL-LHC in the effective field theory approach*, [[arXiv:1801.06093](#)].
- [44] D. Gonçalves, T. Han, F. Kling, T. Plehn, and M. Takeuchi, *Higgs Pair Production at Future Hadron Colliders: From Kinematics to Dynamics*, [[arXiv:1802.04319](#)].
- [45] O. J. P. Eboli, G. C. Marques, S. F. Novaes, and A. A. Natale, *Twin Higgs Boson Production*, *Phys. Lett.* **B197** (1987) 269.
- [46] E. W. N. Glover and J. J. van der Bij, *Higgs Boson Pair Production via Gluon Fusion*, *Nucl. Phys.* **B309** (1988) 282.
- [47] T. Plehn, M. Spira, and P. M. Zerwas, *Pair production of neutral Higgs particles in gluon-gluon collisions*, *Nucl. Phys.* **B479** (1996) 46–64, [[hep-ph/9603205](#)]. [Erratum: *Nucl. Phys.*B531,655(1998)].
- [48] S. Dawson, S. Dittmaier, and M. Spira, *Neutral Higgs boson pair production at hadron colliders: QCD corrections*, *Phys. Rev.* **D58** (1998) 115012, [[hep-ph/9805244](#)].
- [49] R. Frederix, S. Frixione, V. Hirschi, F. Maltoni, O. Mattelaer, P. Torrielli, E. Vryonidou, and M. Zaro, *Higgs pair production at the LHC with NLO and parton-shower effects*, *Phys. Lett.* **B732** (2014) 142–149, [[arXiv:1401.7340](#)].
- [50] F. Maltoni, E. Vryonidou, and M. Zaro, *Top-quark mass effects in double and triple*

- Higgs production in gluon-gluon fusion at NLO*, *JHEP* **11** (2014) 079, [[arXiv:1408.6542](#)].
- [51] J. Grigo, J. Hoff, K. Melnikov, and M. Steinhauser, *On the Higgs boson pair production at the LHC*, *Nucl. Phys.* **B875** (2013) 1–17, [[arXiv:1305.7340](#)].
 - [52] J. Grigo, K. Melnikov, and M. Steinhauser, *Virtual corrections to Higgs boson pair production in the large top quark mass limit*, *Nucl. Phys.* **B888** (2014) 17–29, [[arXiv:1408.2422](#)].
 - [53] J. Grigo, J. Hoff, and M. Steinhauser, *Higgs boson pair production: top quark mass effects at NLO and NNLO*, *Nucl. Phys.* **B900** (2015) 412, [[arXiv:1508.00909](#)].
 - [54] G. Degrandi, P. P. Giardino, and R. Gröber, *On the two-loop virtual QCD corrections to Higgs boson pair production in the Standard Model*, *Eur. Phys. J.* **C76** (2016), no. 7 411, [[arXiv:1603.00385](#)].
 - [55] D. de Florian and J. Mazzitelli, *Two-loop virtual corrections to Higgs pair production*, *Phys. Lett.* **B724** (2013) 306–309, [[arXiv:1305.5206](#)].
 - [56] D. de Florian and J. Mazzitelli, *Higgs Boson Pair Production at Next-to-Next-to-Leading Order in QCD*, *Phys. Rev. Lett.* **111** (2013) 201801, [[arXiv:1309.6594](#)].
 - [57] D. de Florian, M. Grazzini, C. Hanga, S. Kallweit, J. M. Lindert, P. Maierhöfer, J. Mazzitelli, and D. Rathlev, *Differential Higgs Boson Pair Production at Next-to-Next-to-Leading Order in QCD*, *JHEP* **09** (2016) 151, [[arXiv:1606.09519](#)].
 - [58] D. Y. Shao, C. S. Li, H. T. Li, and J. Wang, *Threshold resummation effects in Higgs boson pair production at the LHC*, *JHEP* **07** (2013) 169, [[arXiv:1301.1245](#)].
 - [59] D. de Florian and J. Mazzitelli, *Higgs pair production at next-to-next-to-leading logarithmic accuracy at the LHC*, *JHEP* **09** (2015) 053, [[arXiv:1505.07122](#)].
 - [60] S. Borowka, N. Greiner, G. Heinrich, S. Jones, M. Kerner, J. Schlenk, U. Schubert, and T. Zirke, *Higgs Boson Pair Production in Gluon Fusion at Next-to-Leading Order with Full Top-Quark Mass Dependence*, *Phys. Rev. Lett.* **117** (2016), no. 1 012001, erratum *ibid* 079901, [[arXiv:1604.06447](#)].
 - [61] S. Borowka, N. Greiner, G. Heinrich, S. P. Jones, M. Kerner, J. Schlenk, and T. Zirke, *Full top quark mass dependence in Higgs boson pair production at NLO*, *JHEP* **10** (2016) 107, [[arXiv:1608.04798](#)].
 - [62] G. Ferrera and J. Pires, *Transverse-momentum resummation for Higgs boson pair production at the LHC with top-quark mass effects*, *JHEP* **02** (2017) 139, [[arXiv:1609.01691](#)].
 - [63] G. Heinrich, S. P. Jones, M. Kerner, G. Luisoni, and E. Vryonidou, *NLO predictions*

for Higgs boson pair production with full top quark mass dependence matched to parton showers, *JHEP* **08** (2017) 088, [[arXiv:1703.09252](#)].

- [64] S. Jones and S. Kuttimalai, *Parton Shower and NLO-Matching uncertainties in Higgs Boson Pair Production*, *JHEP* **02** (2018) 176, [[arXiv:1711.03319](#)].
- [65] R. Gröber, A. Maier, and T. Rauh, *Reconstruction of top-quark mass effects in Higgs pair production and other gluon-fusion processes*, *JHEP* **03** (2018) 020, [[arXiv:1709.07799](#)].
- [66] J. Davies, G. Mishima, M. Steinhauser, and D. Wellmann, *Double-Higgs boson production in the high-energy limit: planar master integrals*, *JHEP* **03** (2018) 048, [[arXiv:1801.09696](#)].
- [67] M. Grazzini, G. Heinrich, S. Jones, S. Kallweit, M. Kerner, J. M. Lindert, and J. Mazzitelli, *Higgs boson pair production at NNLO with top quark mass effects*, *JHEP* **05** (2018) 059, [[arXiv:1803.02463](#)].
- [68] R. Gröber, M. Mühlleitner, M. Spira, and J. Streicher, *NLO QCD Corrections to Higgs Pair Production including Dimension-6 Operators*, *JHEP* **09** (2015) 092, [[arXiv:1504.06577](#)].
- [69] R. Gröber, M. Mühlleitner, and M. Spira, *Higgs Pair Production at NLO QCD for CP-violating Higgs Sectors*, *Nucl. Phys.* **B925** (2017) 1–27, [[arXiv:1705.05314](#)].
- [70] D. de Florian, I. Fabre, and J. Mazzitelli, *Higgs boson pair production at NNLO in QCD including dimension 6 operators*, *JHEP* **10** (2017) 215, [[arXiv:1704.05700](#)].
- [71] A. Carvalho, M. Dall’Osso, T. Dorigo, F. Goertz, C. A. Gottardo, and M. Tosi, *Higgs Pair Production: Choosing Benchmarks With Cluster Analysis*, *JHEP* **04** (2016) 126, [[arXiv:1507.02245](#)].
- [72] A. Carvalho, M. Dall’Osso, P. De Castro Manzano, T. Dorigo, F. Goertz, M. Gouzevich, and M. Tosi, *Analytical parametrization and shape classification of anomalous HH production in the EFT approach*, [arXiv:1608.06578](#).
- [73] A. Carvalho, F. Goertz, K. Mimasu, M. Gouzevitch, and A. Aggarwal, *On the reinterpretation of non-resonant searches for Higgs boson pairs*, [arXiv:1710.08261](#).
- [74] G. Buchalla, O. Cata, A. Celis, M. Knecht, and C. Krause, *Complete One-Loop Renormalization of the Higgs-Electroweak Chiral Lagrangian*, *Nucl. Phys.* **B928** (2018) 93–106, [[arXiv:1710.06412](#)].
- [75] **SLD Electroweak Group, DELPHI, ALEPH, SLD, SLD Heavy Flavour Group, OPAL, LEP Electroweak Working Group, L3 Collaboration, S. Schael et al.**, *Precision electroweak measurements on the Z resonance*, *Phys. Rept.* **427** (2006) 257–454, [[hep-ex/0509008](#)].

- [76] G. Buchalla, O. Cata, A. Celis, and C. Krause, *Note on Anomalous Higgs-Boson Couplings in Effective Field Theory*, *Phys. Lett.* **B750** (2015) 298–301, [[arXiv:1504.01707](#)].
- [77] **LHC Higgs Cross Section Working Group** Collaboration, D. de Florian et al., *Handbook of LHC Higgs Cross Sections: 4. Deciphering the Nature of the Higgs Sector*, [arXiv:1610.07922](#).
- [78] N. Deuschmann, C. Duhr, F. Maltoni, and E. Vryonidou, *Gluon-fusion Higgs production in the Standard Model Effective Field Theory*, *JHEP* **12** (2017) 063, [[arXiv:1708.00460](#)]. [Erratum: JHEP02,159(2018)].
- [79] G. Cullen, N. Greiner, G. Heinrich, G. Luisoni, P. Mastrolia, G. Ossola, T. Reiter, and F. Tramontano, *Automated One-Loop Calculations with GoSam*, *Eur. Phys. J.* **C72** (2012) 1889, [[arXiv:1111.2034](#)].
- [80] G. Cullen et al., *GoSam-2.0: a tool for automated one-loop calculations within the Standard Model and beyond*, *Eur. Phys. J.* **C74** (2014), no. 8 3001, [[arXiv:1404.7096](#)].
- [81] C. Degrande, C. Duhr, B. Fuks, D. Grellscheid, O. Mattelaer, and T. Reiter, *UFO - The Universal FeynRules Output*, *Comput. Phys. Commun.* **183** (2012) 1201–1214, [[arXiv:1108.2040](#)].
- [82] A. Alloul, N. D. Christensen, C. Degrande, C. Duhr, and B. Fuks, *FeynRules 2.0 - A complete toolbox for tree-level phenomenology*, *Comput. Phys. Commun.* **185** (2014) 2250–2300, [[arXiv:1310.1921](#)].
- [83] S. Catani and M. H. Seymour, *A General algorithm for calculating jet cross-sections in NLO QCD*, *Nucl. Phys.* **B485** (1997) 291–419, [[hep-ph/9605323](#)]. [Erratum: Nucl. Phys.B510,503(1998)].
- [84] Z. Nagy, *Next-to-leading order calculation of three jet observables in hadron hadron collision*, *Phys. Rev.* **D68** (2003) 094002, [[hep-ph/0307268](#)].
- [85] G. P. Lepage, *VEGAS: An Adaptive Multidimensional Integration Program*, *CLNS-80/447* (1980).
- [86] T. Hahn, *CUBA: A Library for multidimensional numerical integration*, *Comput. Phys. Commun.* **168** (2005) 78–95, [[hep-ph/0404043](#)].
- [87] A. D. Martin, W. J. Stirling, R. S. Thorne, and G. Watt, *Parton distributions for the LHC*, *Eur. Phys. J.* **C63** (2009) 189–285, [[arXiv:0901.0002](#)].
- [88] J. Butterworth et al., *PDF4LHC recommendations for LHC Run II*, *J. Phys.* **G43** (2016) 023001, [[arXiv:1510.03865](#)].
- [89] S. Dulat, T.-J. Hou, J. Gao, M. Guzzi, J. Huston, P. Nadolsky, J. Pumplin, C. Schmidt, D. Stump, and C. P. Yuan, *New parton distribution functions from a*

- global analysis of quantum chromodynamics*, *Phys. Rev.* **D93** (2016), no. 3 033006, [[arXiv:1506.07443](#)].
- [90] L. A. Harland-Lang, A. D. Martin, P. Motylinski, and R. S. Thorne, *Parton distributions in the LHC era: MMHT 2014 PDFs*, *Eur. Phys. J.* **C75** (2015), no. 5 204, [[arXiv:1412.3989](#)].
 - [91] NNPDF Collaboration, R. D. Ball et al., *Parton distributions for the LHC Run II*, *JHEP* **04** (2015) 040, [[arXiv:1410.8849](#)].
 - [92] A. Buckley, J. Ferrando, S. Lloyd, K. Nordström, B. Page, M. Rüfenacht, M. Schönherr, and G. Watt, *LHAPDF6: parton density access in the LHC precision era*, *Eur. Phys. J.* **C75** (2015) 132, [[arXiv:1412.7420](#)].
 - [93] ATLAS Collaboration, G. Aad et al., *Measurements of the Higgs boson production and decay rates and coupling strengths using pp collision data at $\sqrt{s} = 7$ and 8 TeV in the ATLAS experiment*, *Eur. Phys. J.* **C76** (2016), no. 1 6, [[arXiv:1507.04548](#)].
 - [94] CMS Collaboration, *Combined measurements of the Higgs boson’s couplings at $\sqrt{s} = 13$ TeV*, Tech. Rep. CMS-PAS-HIG-17-031, CERN, Geneva, 2018.
 - [95] CMS Collaboration, C. Collaboration, *Combination of searches for Higgs boson pair production in proton-proton collisions at $\sqrt{s} = 13$ TeV*, .
 - [96] ATLAS Collaboration, M. Aaboud et al., *Search for pair production of Higgs bosons in the $b\bar{b}b\bar{b}$ final state using proton-proton collisions at $\sqrt{s} = 13$ TeV with the ATLAS detector*, [arXiv:1804.06174](#).
 - [97] CMS Collaboration, A. M. Sirunyan et al., *Search for Higgs boson pair production in the $\gamma\gamma b\bar{b}$ final state in pp collisions at $\sqrt{s} = 13$ TeV*, [arXiv:1806.00408](#).
 - [98] ATLAS Collaboration, M. Aaboud et al., *Search for Higgs boson pair production in the $\gamma\gamma b\bar{b}$ final state with 13 TeV pp collision data collected by the ATLAS experiment*, [arXiv:1807.04873](#).
 - [99] CMS Collaboration, A. M. Sirunyan et al., *Observation of $t\bar{t}H$ production*, *Phys. Rev. Lett.* **120** (2018), no. 23 231801, [[arXiv:1804.02610](#)].
 - [100] ATLAS Collaboration, M. Aaboud et al., *Observation of Higgs boson production in association with a top quark pair at the LHC with the ATLAS detector*, [arXiv:1806.00425](#).
 - [101] C. Arzt, M. B. Einhorn, and J. Wudka, *Patterns of deviation from the standard model*, *Nucl. Phys.* **B433** (1995) 41–66, [[hep-ph/9405214](#)].
 - [102] G. Buchalla, O. Cata, A. Celis, and C. Krause, *Comment on "Analysis of General Power Counting Rules in Effective Field Theory"*, [arXiv:1603.03062](#).

- [103] A. Manohar and H. Georgi, *Chiral Quarks and the Nonrelativistic Quark Model*, *Nucl. Phys.* **B234** (1984) 189–212.
- [104] E. Bagnaschi, G. Degrossi and R. Gröber, *Higgs boson pair production at NLO in the POWHEG approach and the top quark mass uncertainties*, *Eur. Phys. J. C* **83** (2023) 1054, [[2309.10525](#)].
- [105] G. Buchalla, M. Capozzi, A. Celis, G. Heinrich and L. Scyboz, *Higgs boson pair production in non-linear Effective Field Theory with full m_t -dependence at NLO QCD*, *JHEP* **09** (2018) 057, [[1806.05162](#)].